Petrological and geochemical characteristics of xylites and associated lipids from the First Lusatian lignite seam (Konin Basin, Poland): implications for floral sources, decomposition and environmental conditions

Achim Bechtel[a*], Marek Widera[b], Andreas Lücke[c], Doris Groß[a], Michał Woszczyk[d]

[a] *Montanuniversitaet Leoben, Austria, Department of Applied Geosciences and Geophysics, Peter-Tunner-Str. 5, A-8700 Leoben, Austria*

[b] *Adam Mickiewicz University, Institute of Geology, 12 Krygowski Street, 61-680 Poznań, Poland*

[c] *Forschungszentrum Jülich GmbH, Institute of Bio- and Geosciences, Agrosphere (IBG-3), Wilhelm-Johann-Straße, D-52428 Jülich, Germany*

[d] *Adam Mickiewicz University, Laboratory of Biogeochemistry, 10 Krygowski Street, 61-680 Poznań, Poland*

* Corresponding author. *E-mail address:* Achim.Bechtel@unileoben.ac.at (A. Bechtel)

Abstract

Single pieces of fossil wood fragments (xylites) were collected from the middle Miocene First Lusatian lignite seam at the Adamów, Jóźwin IIB and Tomisławice opencast mines and are characterized by maceral variety, cellulose contents and their molecular and isotopic composition. Biomarker composition of xylites and $\delta^{13}C$ of their total organic matter, lipids and cellulose are used to provide insights into woody plant community and the effects of wood decomposition.

The investigated xylites represent fragments of fossil wood from conifers, most likely species of Cupressaceae, indicated by terpenoid biomarkers characteristic for conifers and by the $\delta^{13}C$ values of the extracted cellulose. This conclusion is confirmed by paleobotanical data highlighting *Taxodium* and *Nyssa* as the main elements of the wet forest swamps. Due to the wet swamp habitat and the

higher-decay resistance exclusively wood fragments of conifers are found in the lignite seam. Minor abundances of angiosperm-derived triterpenoids in the xylites are explained by impurities from inherent detritic lignite.

The xylites are characterized by minor to moderate extents of gelification, but elevated to high cellulose decomposition. The relationship between $\delta^{13}C$ values of xylites and their cellulose contents reflects wood decomposition removing preferentially the ^{13}C-enriched compounds, but decomposition did not affect the $\delta^{13}C$ of cellulose. Despite of similar $\delta^{13}C$ of xylites and detritic lignite, differences in isotopic composition of hopanoids argue for slightly different microbial communities involved in the decomposition of the respective OM. Thus, we conclude that wood decomposition proceeded in a freshwater environment under acidic conditions by fungi and bacteria.

Variations in water availability during growth periods of the conifers are suggested as the most probable cause for the observed minor variations in isotopic composition of plant lipids. The positive relationship found between $\delta^{2}H$ and $\delta^{13}C$ of plant biomarkers, and cellulose of xylites can be explained by the ability of vascular plants to minimize evapotranspiration during dryer phases resulting in plant OM enriched in ^{13}C and ^{2}H. The significant differences in $\delta^{2}H$ between diterpenoids of different structural types and *n*-alkanes are most likely caused by differences in isotopic fractionation during lipid biosynthesis.

Keywords: Biomarkers; Cellulose; Fossil wood; Paleovegetation; Stable isotopes; Terpenoids

1. Introduction

Information about environmetal changes over Earth´s history (e.g., air temperature, humidity, pCO_2, $\delta^{13}C$ of atmospheric CO_2) have been obtained from the stable isotope composition of cellulose extracted from single tree rings and wood fragments (Feng and Epstein, 1995; Schleser, 1995; Arens et al., 2000). However, their interpretation with respect to climate change is complicated by interfering processes like inter-species and intra-species variations in $\delta^{13}C$ and postdepositional changes due to

different decay resistance of macromolecules (Benner et al., 1987; Lücke et al, 1999; van Bergen and Poole, 2002; Marynowski et al., 2007). The combination of biomarker and stable isotope analyses has been successfully applied to reconstruct changes in vegetation and the environment of lignite deposition (van Bergen and Poole, 2002; Poole et al., 2006; Bechtel et al., 2008), as well as in carbon cycling and isotope fractionation processes (Bechtel et al., 2008; Jahren and Sternberg, 2008).

The $\delta^{13}C$ values of individual lipids are frequently used to identify their biological sources and biosynthetic pathways during synthesis (Pancost et al., 2007; Đoković et al., 2018). In a recently published database from peats , biomarkers were related to climate and changes in vegetation (Naafs et al., 2019). Vascular plants adjust stomatal aperture to minimize water loss during warm and dry periods (van Bergen and Poole, 2002; Jahren and Sternberg, 2008; Bechtel et al., 2008) which also affects the isotopic composition of newly formed biomolecules. Therefore, ^{13}C-enriched OM (i.e., cellulose, *n*-alkanes, and diterpenoids) of xylites may indicate dryer conditions during wood formation (and vice versa). The additional influences of environmental and vegetational changes on the molecular and isotopic systematics of modern plants and plant-derived lipids were addressed by Diefendorf and Freimuth (2017) and Diefendorf et al. (2019). Further postdepositonal effects like the effect of increasing maturation on the isotopic composition of lignin (Lee et al., 2019) have also to be considered.

Hydrogen isotope analyses on lipids have been shown to shade light on influences of climatic factors on $\delta^{13}C$ of plant biomarkers. The hydrogen isotopic composition of water in the environment mainly depends on temperature, evaporation and precipitation. The $\delta^{2}H$ values of individual lipids have been shown to reflect the isotopic composition of the source water modified by isotopic fractionation during the biogeochemical pathway (Sessions et al., 1999). Previous studies by Yang and Huang (2003) revealed a similar difference between $\delta^{2}H$ values of alkanes from angiosperm leaves from the Miocene Clarkia deposit (USA) and sediment water (apparent fractionation) as observed in modern species (123‰; Sachse et al., 2004, 2006). Therefore, hydrogen isotope ratios of leaf wax-derived *n*-alkanes are frequently used in paleohydrology and climate research (Sachse et al., 2012).

Our study is focused on the fossil wood remains (xylites) collected from the First Lusatian lignite seam of the Konin Basin in Poland, deposied during the mid-Miocene Climatic Optimum. Based on the results of previous investigations, grasses and herbs were suggested as the peat-forming vegetation of detritic lignites, whereas xylitic lignites showed geochemical characteristics typical of woody conifers (Fabiańska and Kurkiewicz, 2013). This interpretation was supported by biomarker and $\delta^{13}C$ data from xylites of the Lubstów mine within the Konin Basin (Bechtel et al., 2007). Changes in biomarker composition and $\delta^{13}C$ of xylite from the Lubstów mine, related to gelification and cellulose decomposition of wood remains, have also been found (Bechtel et al., 2007).

Palynomorphs of taxa representing a swamp forest environment (*Taxodium*, *Nyssa*, *Alnus* and *Liquidambar*) as well as of shrubs from peat bogs have been found within the lignite seams of the Konin Basin. Pollen elements of the coniferous (e.g., *Sequoia, Pinus*) and deciduous forest (e.g., *Betula*, *Fagus*, *Quercus* and *Ulmus*) indicated the presence of dryer habitats within the mire (Sadowska and Giża, 1991; Piwocki and Ziembińska-Tworzydło, 1997; Kasiński and Słodkowska, 2016; Worobiec et al., 2020). In a previous study, detritic lignite samples from identical sampling locations as the xylites, studied here, (i.e., three opencast deposits within the Konin Basin) have been investigated by Bechtel et al. (2019). The discussion of the lipid composition and carbon isotope data of detritic lignite in combination with the results of paleobotanical studies highlighted the varying contribution of gymnosperms vs. angiosperms to the peat-forming vegetation. Furthermore, the possible contribution of biomarker data to gain information on climate and implications about the effects of changes in vegetation and carbon cycling on $\delta^{13}C$ of lignite samples within the peat have been addressed.

In this study, single pieces from larger xylites were selected from the middle Miocene First Lusatian lignite seam at approximately equal distances along profiles from the same opencast mines within the Konin Basin as investigated for detritic lignite samples in our previous study (Bechtel et al., 2019). The aim of the study is to reveal information about the effects of wood decomposition and environmental conditions on stable isotope composition of woody plant OM. Carbon and hydrogen isotope ratios of cellulose, plant wax and resinous lipids are reported, and are discussed for their

suitability as environmental proxies. Finally, we aim for an improved understanding of palaeoenvironmental changes during peat accumulation from our combined application of molecular and isotopic proxies.

2. Geological setting and samples

Cenozoic sediments were deposited within fault-bounded, relatively shallow tectonic, graben-like depressions located in the Konin vicinity in central Poland (Fig 1a). The Cretaceous bedrock of these grabens is built of marls and sandstones with carbonate cement. The Paleogene and Neogene deposits are characterized by stratigraphic gaps in the territories of the Adamów, Jóźwin IIB and Tomisławice opencasts (Fig. 1). Almost the entire Paleocene, Eocene and upper Oligocene sediments are missing in the record. Therefore, the oldest Paleogene sediments are of early Oligocene age in the Adamów and Tomisławice. They are of marine origin including glauconitic sands and occasionally gravels (Widera, 2010, 2016). It is worth noting that the Paleogene sediments in the area of the Jóźwin IIB opencast have not been documented until now (Chomiak et al., 2019; Widera et al., 2019).

The Koźmin and Poznań formations are the two main Neogene lithostratigraphic units in central Poland. They were deposited after regional uplift of the study area that took place in the late Oligocene. The lower Koźmin Formation is made up of fluvial sands with coaly interbeddings of early- to mid-Miocene age. The upper Poznań Formation, which age covers the time interval from mid-Miocene to early Pliocene, is divided into the Grey Clays and Wielkopolska members (e.g., Piwocki and Ziembińska-Tworzydło, 1997; Widera, 2013; Chomiak et al., 2019; Widera et al., 2019).

The Grey Clays Member consists primarily of the First Lusatian lignite seam, which is currently being exploited in all opencasts belonging to the Konin Basin. This seam is up to several meters thick (on average below 10 m) (Fig. 1b-d) and has been deposited during the final phase of the mid-Miocene Climatic Optimum (Zachos et al., 2001; Bruch et al., 2007; Kasiński and Słodkowska, 2016; Widera, 2016). The age of the studied seam was estimated at 15 +/- 1.5 Ma on the basis of radiometric dating of tuff layers from various regions of Poland, including the Konin area (Wagner, 1984; Matl and Wagner, 1985). Additionally, this lignite seam is correlated palynologically both throughout the Polish

and European lowlands territory (e.g., Sadowska and Giża, 1991; Kasiński and Słodkowska, 2016; Worobiec et al., 2020). The First Lusatian lignite seam evolved from low-lying mires (backswamps) in the extra-channel area of a mid-Miocene fluvial system (Widera, 2016; Chomiak et al., 2019).

The examined lignite seam (i.e., the First Lusatian one) belongs to humic ortholignite. It is characterized by low-coal rank (mean reflectance (R_r^o) < 0.3%) and low carbon content (60% < C^{daf} < 70%) (Kwiecińska and Wagner, 2001). Moreover, a relatively high ash yield (A^d ~ 20 wt% average) and low average sulfur content (< 1 wt%) are typical of the First Lusatian lignite seam in the Konin Basin and in the remaining part of central Poland (e.g., Piwocki, 1987; Kwiecińska and Wagner, 1997). Twenty-seven samples of large pieces of xylite, carefully separated from the detritic lignite, were taken along three profiles at the Adamów, Jóźwin IIB and Tomisławice opencasts (Fig. 1). The location of sampling is shown in Fig. 1b-d.

3. Analytical methods

3.1. Micropetrography

Twelve xylite samples from different parts of the three profiles have been selected for microscopic inspection based on variying cellulose yields. Pieces from homogenised xylite samples were embedded into epoxy resin and polished to obtain a smooth surface. The samples were investigated by a Leica DM 4P microscope using reflected white and fluorescent light.

3.2. Ash yield, carbon, and total sulfur analyses

The total carbon (TC), and total sulfur (TS) contents were determined by Elemental Analysis (Eltra Helios CS analyser). Total organic carbon (TOC) was measured with the same instrument on samples pre-treated with half-concentrated phosphoric acid. The total inorganic carbon (TIC) was calculated as TIC [wt%] = TC-TOC. Ash content was determined via combustion of dried and homogenized samples at 550°C for 4 h.

3.3. Pretreatment and cellulose extraction

160 Pieces of fossil wood were freeze-dried and milled for homogenization. An aliquot of the sample was
161 decalcified in a water bath (5% HCl, 50°C) for two hours to remove inorganic carbonates prior to the
162 analyses of $\delta^{13}C$ of fossil wood. Cellulose extraction followed the CUAM-protocol (Wissel et al.,
163 2008) with slight adaptations for the specific samples.
164
165 *3.4. Stable carbon isotope analyses*
166 For $\delta^{13}C$ analyses of fossil wood and cellulose, a sample amount of about 200–300 µg (~ 100 µg
167 carbon) was weighed into tin foil capsules. Samples were combusted at 1050°C with excess oxygen in
168 an elemental analyser (EuroEA, Eurovector) and measured online with a coupled isotope ratio mass
169 spectrometer (IsoPrime, GV-Instruments). Carbon content was determined by peak integration (*m/z* 44
170 and 45) and calibrated against a certified elemental standard.
171 Isotope ratios are given as δ-values in per mil (‰), where $\delta = (R_{sample}/R_{standard}-1) \times 1000$, with
172 R_{sample} and $R_{standard}$ as isotope ratios ($^{13}C/^{12}C$) of sample and standard, respectively. Samples were
173 measured together with laboratory standards calibrated against international carbon isotope standards
174 and are reported scale-normalized to the VPDB scale. The overall precision of replicate analyses was
175 better than ±0.1‰. Preparation of cellulose and carbon isotope measurements on fossil wood and
176 cellulose were carried out at the Institute of Bio- and Geoscience, Agrosphere, Forschungszentrum
177 Jülich GmbH (Germany).
178
179 *3.5. Molecular composition of lipids*
180 After extraction of aliquots (5 g) of dry lignite samples by a mixture (9:1) of dichloromethane
181 (DCM) and methanol (MeOH) in a Dionex ASE 200 accelerated solvent extractor (75°C, 100 bar, 1 h),
182 the extracts were saponified at 80°C for 3 h using a 6% potassium hydroxide (KOH) solution in
183 MeOH. The neutral lipids were recovered by extracting the KOH/MeOH with 3 x 1 ml *n*-hexane,
184 whereas fatty acids were subsequently recovered after addition of concentrated HCl at pH=1. The
185 neutral lipids were then separated using Supelco silica columns (LC-SI, 6 ml, 500 mg sorbent) into 3
186 fractions of various polarity using 4 mL of the following eluents: 1) 100% *n*-hexane; 2) *n*-hexane:

DCM mixture (1:1 v/v) and 3) DCM:MeOH mixture (95:5 v/v). The first fraction (F1) contains hydrocarbons, the second ones (F2) ketones plus polycyclic aromatic hydrocarbons, and the third fraction (F3) contains the alcohols. Fatty acids (FAs) and fractions F3 were derivatised with BSTFA (N,O-bis(trimethylsilyl)trifluoroacetamide) for 1 h at 80°C to form trimethylsilyl (TMS) esters and ethers, respectively.

For gas chromatographic analysis 2 µl of the fractions was injected slitless (injector temperature 275°C) onto a 60 m DB-5MS fused silica column (i.d., 0.25 mm; 0.25 mm film thickness). The gas chromatograph (GC) was coupled to a ThermoFisher ISQ quadrupole mass spectrometer (GC–MS system). The instrumental parameters during analyses were identical to that outlined in our previous article (Bechtel et al., 2019). Data were processed using an Xcalibur data system. Individual compounds were identified on the basis of retention time and by comparison of the mass spectra with published data. Concentrations of different compounds were calculated using peak areas in the total ion current chromatograms in relation to those of internal standards added in known concentrations (squalane to F1, 1,1´-binaphthyl to F2, 1-nonadecanol to F3, and nonadecanoic acid to FA fractions, respectively). The concentrations are given relative to the TOC contents of the xylites.

3.6. Compound-specific isotope analyses

The $\delta^{13}C$ and $\delta^{2}H$ of *n*-alkanes and terpenoids were measured in duplicate, using a Trace GC-Ultra gas chromatograph attached to a Thermo Fischer Delta-V isotope ratio mass spectrometer (irMS) via a combustion and high temperature reduction interface, respectively (GC Isolink, Thermo Fischer). The GC was equipped with a 30 m DB-5MS fused silica capillary column (i.d., 0.25 mm; 0.25 µm film thickness). The GC operational parametrers were identical to that described by Bechtel et al. (2019). Raw isotope values were initially converted to the VPDB and VSMOW scale, respectively, using Thermo Isodat 3.0 software and pulses of a monitoring gas measured at the beginning and end of each analysis. Analytical precision (between ±0.2 and 0.3‰ for C; below ±3‰ for H) was controlled by repeated measurements (after every 10 sample injections) of the C3 *n*-alkane standard mix from Arndt Schimmelmann (Indiana University).

4. Results

4.1. Micropetrography and bulk geochemical data

Microscopic inspection of selected xylites was performed to evaluate the purity of the macrofossils and their degree of gelification. The samples contain mainly textinite, textoulminite, and phlobaphinite in various proportions. Inside the cells of textinite, crystalline inorganic phases (Fig. 2a) are observed in several samples. Increased extents of gelification are reflected by higher textoulminite and lower textinite abundances (Table 1). Textinite is the predominant maceral in ungelified samples (Fig. 2a–d), whereas gelified samples contain textoulminite plus rare ulminite (Fig. 2e, f). Lower fluorescence intensities of huminite (dark brownish to greenish) are observed in gelified xylites (Table 1; Fig. 2). Generally, xylites from the Jóźwin IIB mine are characterized by higher extents of gelification (Table 1). Resinite is present in minor amounts in all xylites (Fig. 2a, b).

The TOC contents of fossil wood remains are in the range of 32.5 to 53.6 wt% (Table 1). The TOC values are lower than previously obtained from the xylites of the Lubstów deposit, despite of comparable extents of gelification (Bechtel et al., 2007). Low TOC contents (< 40 wt%) were obtained from the lowermost sample taken from the Tomisławice mine, in sample JX-02 from the Jóźwin IIB mine and from several xylites of the Adamów mine (Fig. 3a). Ash yields of several of the woody macrofossils are exceeding 5 wt% (Table 1; Fig. 3a), arguing for impurities due to inherent detritic lignite, as wood from temperate zones yielded less than 1 wt% ash (Misra et al., 1993). Ash yields up to 5 wt% are reported from tropical wood (Fengel and Wegener, 1984). The TOC of woody macrofossils is controlled by interfering parameters, including mineral matter contents from inherent detritic lignite, its TOC content, and cellulose decomposition. Therefore, no relationship exists between ash yields and TOC of xylite.

The TIC contents vary between 0.0 and 3.8 wt% (Table 1; Fig. 3b) and are generally higher as measured within samples of detritic lignite (Bechtel et al., 2019). The results argue for mineralization of wood by calcium carbonate within the mire. Based on the results obtained during experimental

treatments of wood with electrolyte solutions (Merk et al., 2016), the crystalline phases inside the cellular structure of wood (Fig. 2a) consist most likely of $CaCO_3$ polymorphs.

Total sulfur contents below 2 wt% argue for deposition in a freshwater environment (Casagrande, 1987). Elevated sulfur contents are obtained from xylites from the upper part of the Adamów mine, xylites from the Jóźwin IIB mine and the lowermost sample from the seam in the Tomisławice mine (Fig. 3b).

Cellulose yields of fossil wood remains ranged between 1.6 and 24.2% (dry wt.; Table 1; Fig. 3a), but seem to be unrelated to the varying gelification extent of selected samples (Table 1). Highest cellulose yields were measured in xylites of the Tomisławice mine (Fig. 3a). With an approximate original cellulose content of 40 to 50%, (Pettersen, 1984), the data indicate advanced to high extent of cellulose decomposition. However, impurities due to inherent detritic lignite certainly also reduced cellulose yields.

Extractable organic matter yields (EOM) vary from 18.3–64.6 mg/g TOC (Table 1). A negative relationship exists between EOM and cellulose yields (Fig. 4), suggesting biogeochemical formation of lipids in the wood during gelification and cellulose decomposition by bacteria and fungi. However, the relative enrichment of EOM due to the depletion of fossil wood in cellulose and (partly) lignin cannot be excluded. Hydrocarbons plus ketones contribute between 5 and 16% to the EOM, consistent with the low maturity of organic matter. Relative proportions of alcohols (6–15%) and carboxylic acids (9–22% of EOM) vary in comparable ranges. Polar macromolecular compounds (i.e., resins; Table 2) are present in highest proportions (> 50%).

4.2. Molecular composition of wood and associated lipids

As the presence of inherent detritic lignite is indicated based on ash yields, plant-wax lipids, steroids and hopanoids may partly originate from detritic OM, and are only briefly discussed in this paper. A detailed overview of the results from detritic lignite at identical sampling sites within the seam is given by Bechtel et al. (2019). However, the isotopic compositions of *n*-alkanes are expected to provide important supplementary information about the determining role of environmental factors

on $\delta^{13}C$ and $\delta^{2}H$ of lipids from land plants, as plant-wax alkanes have been most extensively studied for the reconstruction of climatic changes (Sachse et al., 2012). They are, therefore, discussed together with the results from resinous compounds and cellulose. Hopanoids are included as they may provide additional information about the environment of wood decomposition and the bacterial communities.

4.2.1. Plant wax derived lipids

The *n*-alkanes contents of the xylite samples vary from 75 to 440 µg/g TOC (Table 2; Fig 3c). The *n*-alkane concentrations of woody macrofossils are unrelated to differences in lithotype within the lignite sections (Fig. 3). Long-chain *n*-alkanes (>*n*-C_{27}; Fig. 5a) with a marked predominance of odd carbon numbered homologues are present in highest abundances, consistent with their origin from plant-wax OM and the immature character of OM (Eglinton and Hamilton, 1967; Cranwell, 1977).

The long-chain (> C_{23}) odd-numbered *n*-alkan-2-ones are relatively abundant in the ketones fractions (F2) and occur together with polycyclic aromatic and polar terpenoids Fig. 5b). The 6,10,14-trimethyl-pentadecan-2-one is present in high abundances and is suggested to represent a degradation product of phytol (Fig. 5b).

The alcohol fractions (F3) of the samples are dominated by *n*-alkanols in the C_{14}–C_{30} carbon number range (Fig. 5c). Predominant are the even-numbered long-chain *n*-alkanols (> C_{22}), originating from plant cuticular waxes (Püttmann and Bracke, 1995; Ficken et al., 2000).

Even-numbered saturated fatty acids (*n*-FAs) with maxima at C_{24} and C_{26}, respectively, predominate in all xylite samples (Fig. 5d). They are characteristic constituents of leaf epicuticular waxes (Eglinton and Hamilton, 1967). Beside of hopanoids, microbial activity during gelification of the woody macrofossils is reflected by low relative abundances of branched-chain FAs ($C_{16:1}$ and $C_{18:1;}$ Fig. 5d) (Volkman et al., 1980; Kaneda, 1991).

4.2.2. Steroids, hopanoids

The C_{29} (Δ^4, Δ^5)-sterenes and C_{29} diaster-13(17)-enes were found in low concentrations (4.1–48.9 µg/g TOC, Table 2). In contrast, β-sitosterol, campesterol, stigmastanol (Fig. 5c), and minor cholesterol (all

as TMS ethers) are present in the alcohol fractions (F3) of several xylites in high abundances (sum of sterols plus stanols > 100 μg/g TOC; Table 2; Fig. 3c). The predominance of C_{29} steroids in the lipids is consistent with their origin from land plant OM (Volkman, 1986).

Hopanoids are found in elevated concentrations in the extracts of the xylites (Table 2; Fig. 3c). The 17α,21β(H)- and 17β,21β(H)-type hopanes from C_{27} to C_{31} were identified. The C_{28} hopanes are missing, and the 17α,21β(H)-C_{31} hopane (22R) predominates by far (Fig. 5a). In addition to the hopanes, the C_{27} and C_{30} hop-17(21)-enes are present. All samples show low ββ/(αβ +ββ) ratios (0.06–0.22) of the C_{31} hopanes (Table 2; Fig. 5a). The D-ring monoaromatic hopanoid occurs in all xylite samples (Philp, 1985). The C_{32} ββ-hopanol (TMS) is present in the alcohol fractions, and C_{31} to C_{32} ββ- and αβ- hopanoic acids (TMS) were identified in the carboxylic acid fractions (FA) in variable abundances (8.8–83.2 μg/g TOC; Figs. 5c, d). Highest concentrations of hopanoids (> 100 μg/g TOC) were found in xylites from the Jóźwin IIB mine (Table 2; Fig. 3c).

4.2.3. Sesquiterpenoids, diterpenoids, non-hopanoid triterpenoids

The sesquiterpenoids consist of cadinenes, curcumene, cuparene and cadalene (3.4–91.5 μg/g TOC) in the hydrocarbon fractions (Grantham and Douglas, 1980; Simoneit and Mazurek, 1982). Cadalene predominates by far (Fig. 5a). Major constituents of the hydrocarbons are abietane, isopimarane, pimarane, and phyllocladane type diterpenoids. Saturated diterpenoids include, isonorpimarane, norpimarane, norabietane, pimarane, abietane, and 16α(H)-phyllocladane (Hagemann and Hollerbach, 1979; Noble et al., 1985; Philp, 1985; Fig. 5a). Pimarane, isonorpimarane, and norpimarane are present in highest abundances in most samples. Aromatic diterpenoids (e.g., dehydroabietane, 18-norabietatriene, tetrahydroretene, simonellite, and retene; Philp, 1985) were identified in the hydrocarbons (F1) and partly the ketones (F2) fractions (Figs. 5a, b). Ferruginol and dehydroferruginol (Otto et al., 1997) are present in the ketones fractions (Fig. 5b) of all samples. Furthermore, labdan-15-oic, isopimaric, and abietic acids (as TMS esters; Otto and Simoneit, 2002) were identified in the carboxylic acids fractions (Fig. 5d). Total concentrations of diterpenoids vary

between 148 and 1698 µg/g TOC (Table 2). High concentrations of diterpenoids indicate abundant resinous organic matter in the fossil wood fragments (Fig. 3d).

In most xylites, the following oleanane, ursane, and lupane type triterpenoids were identified in the hydrocarbon fractions of xylites: *des*-A-oleanenes, *des*-A-lupane, olean-12-ene, olean-13(18)-ene, and urs-12-ene. They are present in very low concentrations between 3.1 and 24.7 µg/g TOC (ten Haven et al., 1992; Logan and Eglinton, 1994; Philp, 1985; Rullkötter et al., 1994). The aromatic triterpenoid hydrocarbons contain of 24,25-dinoroleana-1,3,5(10),12-tetraene (Fig. 5a), 24,25-dinoroleana-1,3,5(10)-triene, 24,25-dinorlupa-1,3,5(10)-triene (Spyckerelle et al., 1977; Wakeham et al., 1980; Wolff et al., 1989), as well as tetramethyl-octahydro-picenes (Fig. 5b) and trimethyl-tetrahydro-picenes (LaFlamme and Hites, 1979; Wakeham et al., 1980). In the ketones (F2) and alcohol fractions (F3), respectively, friedelin, β- and α-amyrin, as well as lupeol were identified, (Fig. 5b, c). Total concentrations of non-hopanoid triterpenoids (17–106 µg/g TOC) are low compared to the contents of diterpenoids (Table 2; Fig., 3d).

4.3. Stable isotope composition of xylites and lipids

The $\delta^{13}C$ values of the xylites (TOC) vary between –23.7 and –26.6‰ (Table 1; Fig. 6a). The average carbon isotopic composition ($\delta^{13}C$ = –25.0‰) is nearly identical as reported for xylites of the Lubstów deposit (mean $\delta^{13}C$ of –24.5‰; Bechtel et al., 2007), The carbon isotopic composition also varies in comparable ranges as obtained from detritic lignite samples from identical sections of the First Lusatian seam in the Konin Basin (–24.9 to –26.2 ‰; Bechtel et al., 2019). Carbon isotope ratios of extracted cellulose are in the range from –19.9 to –22.7‰ (Table 1; Fig 6a). On average $\delta^{13}C$ cellulose is enriched by about 3.6‰ with respect to $\delta^{13}C$ of xylites.

The odd numbered C_{27} to C_{31} *n*-alkanes yielded $\delta^{13}C$ values between −29.0 and −31.5‰ (Table 3) as usually obtained from C3 plants (O'Leary, 1981). As previously found in several lignite and coal samples (e.g., Collister et al., 1994; Huang et al., 1995), a general trend of slightly decreasing $\delta^{13}C$

values with increasing carbon number is observed (Fig. 6b). The hydrogen isotopic compositions of these *n*-alkanes are in the range of −162 to −174‰ (Table 4; Fig. 6d).

The $\delta^{13}C$ values of norabietane, pimarane and 16α(H)-phyllocladane vary between −24.2 and −26.5‰, and are about 4 to 5‰ heavier than those of the *n*-alkanes (Table 3; Fig. 6c). Comparable data have been reported for coals from the Liaohe Basin, China (Tuo et al., 2003). Aromatic diterpenoids (e.g., dehydroabietane, simonellite) show up to 1‰ higher $\delta^{13}C$ (–23.8 to –25.1‰) as saturated diterpenoids (Table 3), in agreement with the results of previous studies (Đoković et al., 2018). Gymnosperm-derived diterpenoids are depleted in ^{2}H compared to long-chain *n*-alkanes (–231 to –294 ‰; Table 4; Fig. 6e). Pimarane-type diterpenoids are characterised by lowest $\delta^{2}H$ values (Table 5).

The isotopic composition ($\delta^{13}C$) of the αβ-C_{31} hopane (22R) fall within the range of –25.6 to –27.9‰; Table 3). Slightly lower $\delta^{13}C$ (−26-6 to −28.6‰) have been obtained from the ββ-C_{31} hopane. In contrast, the $\delta^{13}C$ values of the hop-17(21)-ene vary between −29.3 and −34.4‰ (Table 3).

5. Discussion

5.1. Chemotaxonomy of xylites

Swamp forest taxa in the Konin lignite include *Taxodium, Glyptostrobus*, and *Nyssa*, whereas pollen elements of *Pinus*, *Sequoia*, *Betula*, *Fagus*, *Quercus* and *Ulmus* are considered as are derived from dry forest surrounding the swamps (Sadowska and Giża, 1991; Piwocki and Ziembińska-Tworzydło, 1997; Kasiński and Słodkowska, 2016; Worobiec et al., 2020).

The frequency abundances of different compound classes of terpenoids in the xylite extracts are shown in Fig. 7. Pimarane, abietane and phyllocladane type diterpenoids predominate by far. Ferruginol and dehydroferruginol are present in variable abundances in the xylites (Fig. 7). While diterpenoids have been considered as markers for gymnosperms (i.e., conifers; Otto and Wilde, 2001), oleanane, ursane and lupane type triterpenoids have been reported to occur in angiosperms (Karrer et al., 1977; Sukh Dev, 1989). The percentages of the summed diterpenoids relative to total terpenoids range from 74–99% ((di-/(di- + tri-)terpenoid ratios > 0.73; ratios are based on the sum of

concentrations of non-polar and polar compounds) and, thus, argue for gymnosperms (i.e., conifers) as sources of our sampled wood fragments (Table 2; Fig. 3e). This is consistent with previous data of terpenoid hydrocarbon ratios from xylites of the Second Lusatian lignite seam (Bechtel et al., 2007; Fabiańska and Kurkiewicz, 2013).

As only pieces from single larger xylites have been collected, they should contain the lipids characteristic for either gymnosperm or angiosperm wood. However, impurities from inherent detritic lignite are most likely responsible for the contribution of triterpenoids, as indicated by a negative relationship between ash yields and di-/(di- + tri-)terpenoid ratios (Fig. 8). This implies that the non-specific lipids (plant-wax constituents, steroids, hopanoids) may reflect mixtures from various sources (i.e., wood and detritic lignite).

The relative abundances of terpenoid biomarkers from xylites and detritic lignite differ significantly (Fig. 7; Fig. 8 in Bechtel et al., 2019). The detritus samples contain high amounts of triterpenoids of angiosperm origin, while diterpenoids predominate by far in the extracts from xylites. The results imply different floral assemblages contributing to detritic lignite and the sole occurrence of conifer wood in xylites, respectively. The data argue for the selective preservation of conifer wood in the mires.

The phenolic abietane ferruginol is present in the extracts of most conifer families, especially in species of Cupressaceae, and Podocarpaceae, but seems to be absent in Pinaceae (Otto and Wilde, 2001). Phyllocladanes have been also described to occur in different conifer families; only in Pinaceae, phyllocladanes have not been found. Abietane type diterpenoids in the geosphere are considered to be derived from abietic acid, preferably found in Pinaceae, or from phenolic derivatives (i.e., ferruginol; Otto et al., 1997). Based on palynological and biomarker data from Pliocene lignite deposits of the Yunnan Province (China), abietane, pimarane, and isopimarane have been suggested as markers for Pinaceae (Liu et al., 2018). Considering the age of the Polish lignite, the paleobotanical data from lignites of the Konin Basin, and the terpenoids discussed above, xylites could, thus, more specifically be interpreted as wood remains of species of the coniferales families Cupressaceae, and/or Pinaceae

398 (Otto and Wilde, 2001; Stefanova et al., 2002). Again, this is in accordance with our previous study on
399 xylites from the Lubstów deposit (Bechtel et al., 2007).
400 Diterpenoid composition of detritic lignite (Fig. 8, Bechtel et al., 2019) and xylites (Fig. 7) are
401 comparable showing varying abundances of phyllocladane-, abietane-, pimarane-type diterpenoids and
402 ferruginol plus dehydroferruginol, arguing for their origin from species of Cupressaceae and Pinaceae
403 families. However, the presence of phyllocladane type diterpenoids, ferruginol and cuparene in all
404 samples taken from individual xylites argue against Pinaceae and for Cupressaceae as precursor plants
405 of fossil wood remains (Grantham and Douglas, 1980; Otto and Wilde, 2001). The sole presence of
406 woody fragments from conifers (most probably Cupressaceae) may also be due to their higher-decay
407 resistance compared to angiosperms (Bechtel et al., 2008). Fossil wood from Pinaceae may have not
408 been found due to their occurrence in dryer habitats (Kasiński and Słodkowska, 2016; Worobiec et al.,
409 2020). Selective alteration and degradation of terpenoids during diagenesis must be considered
410 (Diefendorf et al., 2015), but seem to be of minor importance based on low to moderate extent of
411 gelification of xylites and the low maturity of OM.
412
413 *5.2. Environment and mechanisms of wood decomposition*
414 Based on low sulfur contents (< 2 wt%) of the detritic lignite samples (Bechtel et al., 2019) and
415 the investigated xylites (Table 1), an evolution of the lignite seam under freshwater conditions is
416 suggested. Previous palynological and sedimentological analyses provided further evidence for peat
417 formation in the overbank depositional environment typical of backswamp areas (Sadowska and Giża,
418 1991; Piwocki and Ziembińska-Tworzydło, 1997; Widera, 2016).
419 Information about wood decomposition can be derived from hopanoid composition, gelification
420 extent and cellulose yield of the woody macrofossils. Cellulose yields of the xylites between 1.6 and
421 24.2 wt% argue for advanced to high degradation states. Cellulose decomposition has been attributed
422 to the activities of fungi (Benner et al., 1987) under oxic conditions. Nevertheless, bacterial
423 communities have been suggested to likewise contribute to wood decomposition under aerobic and
424 anaerobic conditions (Benner et al., 1984; Bechtel et al., 2007). The enhanced contents of hopanoids

obtained from xylites characterized by low cellulose yields confirm such a bacterial component for our samples (Figs. 3, 9). Larger contributions from impurities with larger decomposition state of the wood could result in a comparable relationship, but can be excluded based on the lack of relationship between hopanoid contents and ash yields. Likewise, increased impurities from detritic lignite, containing decomposed fragments from angiosperm wood, may result in the depletion of cellulose within the xylites. However, hopanoid contents of detritic lignite and xylites vary within comparable ranges (Bechtel et al., 2019) and would not explain the increasesd hopanoid contents in low cellulose xylites.

The hopane derivatives and hop-17(21)-ene found in the xylites are most likely derived from tetrafunctionalized bacteriohopanepolyols and diplopterol, respectively (Brassell et al., 1980; Ourisson et al., 1979; Rohmer et al., 1992; Inglis et al., 2018). These compounds have been identified in bacteria, as well as in some mosses, ferns, lichens and fungi (Bottari et al., 1972; Ourisson et al., 1979; Rohmer and Bisseret, 1994). The results of recent studies provided evidence that in peatlands αβ-hopanoids are acid-catalyzed degradation products (Inglis et al., 2018). Therefore, the ββ/(αβ +ββ) hopane ratio has been used to reconstruct the pH conditions in peat-forming environments. Very low ββ/(αβ +ββ) ratios (0.06–0.22 μg/g TOC ; Table 2) found in the extracts of the xylite fragments, their moderate hopanoid concentrations (34–111 μg/g TOC) and low sulfur contents (average value of 1.2 wt%) point towards wood decomposition in the peat under acidic conditions (Casagrande, 1987; Inglis et al., 2018). The ββ/(αβ +ββ) ratios are similar to the data obtained from detritic lignite samples (between 0.07 and 0.17 μg/g TOC; Bechtel et al., 2019).

5.3. Factors influencing carbon isotopic composition of fossil wood and plant lipids

The positive relationship between cellulose content and $\delta^{13}C$ values of xylites (TOC; Table 1) indicates the progressive depletion of wood in ^{13}C during cellulose decomposition (Fig. 10a), as already reported from previous studies (Benner et al., 1987; Lücke et al., 1999; Bechtel et al., 2007). Our $\delta^{13}C$ data of xylite OM and cellulose (Table 1; Fig. 6a) are consistent with the suggested origin of

xylites from woody conifers, as cellulose from angiosperm wood has been reported to be ^{13}C depleted relative to conifer wood (Lücke et al., 1999). This is also indicated by their terpenoid biomarker composition.

Measurements during artificial maturation of modern wood indicated that during decomposition cellulose is only slightly depleted in ^{13}C (< 0.3‰ relative to untreated wood) in contrast to the whole wood (Schleser et al., 1999). Consistent with these observations, no significant relationship exists between $\delta^{13}C$ of extracted cellulose from the xylite samples and cellulose yields (Fig. 10a). Our data show varying differences in $\delta^{13}C$ of xylites and extracted cellulose between 2.3 and 4.3‰ ($\Delta\delta^{13}C = \delta^{13}C_{xylite} - \delta^{13}C_{cellulose}$) along the expected negative relation between $\Delta\delta^{13}C$ and cellulose yield (Fig. 10b). These isotopic differences are in general agreement with that obtained for Miocene taxodioid Cupressaceae (former Taxodiaceae) wood from the Garzweiler seam in Germany (3.8‰; Lücke et al., 1999) and with isotopic data from fossil wood and extracted cellulose (differences in $\delta^{13}C$ of 3.0 to 4.6‰) from the Second Lusatian lignite seam at the Lubstów deposit (Bechtel et al., 2007).

The isotopic composition ($\delta^{13}C$) of the αβ-C_{31} hopane (22R) was found to be slightly depleted in $\delta^{13}C$ (−25.6 to –27.9‰; Table 3) relative to wood OM (mean $\delta^{13}C$ of TOC of xylites −25.0‰; Table 3; Fig. 6a). The results argue for a heterotrophic bacterial population. The $\delta^{13}C$ values of the ββ-C_{31} hopane (–26.6 to –28.6‰) are on average 1.2‰ lower as the values obtained from αβ-C_{31} hopane. In contrast, the C_{30} hop-17(21)-enes show ^{13}C-depleted isotopic composition (average $\delta^{13}C$ of –32.2‰; Table 3). Overalll, the results imply the contribution of various bacterial communities in the decomposition of wood within the peat (Pancost et al., 2000, 2007; Mitrović et al., 2016). Due to impurities from detritic lignite, the hopanoids could reflect the microbial activities using OM of detritic lignite as substrates. Despite of similar $\delta^{13}C$ values of TOC of xylites and detritic lignite (−25.0 and −25.6‰, respectively), significantly lower $\delta^{13}C$ of ββ-C_{31} hopane (−32.2 to −36.7‰) in the lignite samples at identical sampling positions as the xylites (Bechtel et al., 2019) argue against this possibility. More likely, slightly different microbial communities were involved in the decomposition of OM of xylites (compared to detritic lignite).

The $\delta^{13}C$ of extracted cellulose, plant wax *n*-alkanes (C_{27}, C_{29}, C_{31}), and diterpenoids show minor, but more or less parallel, fluctuations with depth in all 3 profiles (Fig. 6b, c). Because of similar sources of wood macrofossils from conifers (e.g., most likely from Cupressaceae) inter-species variations on $\delta^{13}C$ of cellulose and resinous compounds should be neglectible. The parallel tendencies in $\delta^{13}C$ with depth may argue for variations in $\delta^{13}C$ of CO_2 available to the plants as one of the possible causes. However, $\delta^{13}C$ variations of 2.5‰ are within the range of variability observed in the plants within a habitat, and can be explained without invoking variations in $\delta^{13}C$ of CO_2 (Diefendorf et al. 2019; Inglis et al., 2019). Furthermore, the Mid-Miocene Climatic Optimum is characterized by minor variations in $\delta^{13}C$ values of atmospheric CO_2 (around −5‰; Zachos et al., 2001; Tipple et al., 2010), Therefore, the obtained differences in $\delta^{13}C$ are interpreted to have been caused by water availability to the plants due to the adjustment of stomatal aperture to minimize water loss (van Bergen and Poole, 2002; Jahren and Sternberg, 2008; Bechtel et al., 2008; Diefendorf and Freimuth, 2017; Diefendorf et al., 2019).

5.4. H-isotopic composition of plant lipids and climate

Paleobotanical data from the study area indicated humid conditions (mean annual precipitation in the range 820–1300 mm/year; Ivanow and Worobiec, 2017) and warm mean annual air temperatures (between 15.7–19.7 °C; Kasiński and Słodkowska, 2016; or between 15.7–18.0 °C; Worobiec et al., 2020) during the mid-Miocene Climatic Optimum. Following from this information we would expect only minor variations in the $\delta^{2}H$ values of meteoric water (Bowen, 2008) in the area of the Konin Basin during peat formation. Irrespective of that, variations in the extent of evapotranspiration, as well as biological factors, influence apparent fractionation and can lead to considerable fluctuations in $\delta^{2}H$- of plant wax lipids (Sachse et al., 2006, 2012; Freimuth et al., 2017).

The $\delta^{2}H$ values of *n*-alkanes and diterpenoid biomarkers show variations up to 10‰ within the profiles (Table 4; Fig. 6d, e). Beside of the possible influence of minor climate variations, the low variability of $\delta^{2}H$ values of the *n*-alkanes from plant waxes and diterpenoids from wood resins could

also be caused by changes in water availability during the respective growth period of the trees, modifying apparent H-isotope fractionation through changes in stomatal aperture. This interpretation is supported by the positive relationships between δ^2H and $\delta^{13}C$ values of *n*-C_{29}, and between δ^2H of the *n*-C_{29} alkane and $\delta^{13}C$ of extracted cellulose from the fossil wood fragments (Fig. 11a, b). The influence of different extents of degradation on the related isotopic patterns (δ^2H of *n*-C_{29} and $\delta^{13}C$ of cellulose) can be neglected, as cellulose decomposition did not result in a significant shift in $\delta^{13}C$ of cellulose (see discussion in Chapter 5.3). Furthermore, δ^2H of plant-wax *n*-alkanes are considered to be only influenced during catagenesis over geological time scales (Schimmelmann et al., 2006).

Significant differences in δ^2H are seen between diterpenoids and *n*-alkanes, as well as between diterpenoids of different structural types (Table 4; Fig. 6d, e). This can be explained by differences in isotopic fractionation during lipid biosynthesis, as *n*-alkyl lipids associated with the acetogenic pathway were reported to be less depleted in ^2H as the diterpenoids derived from the non-mevalonic acid pathway (Chikaraishi et al., 2004). Further isotopic fractionation during lipid biosynthesis occurs during various biochemical reactons, such as decarboxylation of pyruvate to form acetate and hydrogenation with NADPH, respectively (Chikaraishi et al., 2004). However, pimarane-type diterpenoids are characterized by very low δ^2H values (around -280‰; Fig. 6e) compared to the abietane- and phyllocladane-type compounds. The results are in agreement with previous data (Tuo et al., 2006) and could be explained by different sources of hydrogen and/or different biosynthetic pathways during formation of pimarane-type diterpenoids.

6. Conclusions

Woody macrofossils (xylites) from the First Lusatian lignite seam are characterized by minor extents of gelification, but elevated to high cellulose decomposition. Based on terpenoid biomarker composition and $\delta^{13}C$ values of extracted cellulose, the xylites are indicated as fragments of fossil wood from conifers. Xylites most likely represent species of Cupressaceae, in agreement with available paleobotanical data. Impurities from inherent detritic lignite are responsible for minor

contributions of angiosperm-derived triterpenoids in the OM of xylites, as lipids from detritic lignite have been found to contain triterpenoid biomarkers in high abundances. Similarly, plant-wax lipids, steroids and hopanoids may be partly derived from OM of detritic lignite. The fact that only woody fragments of conifers have been found is explained by their higher-decay resistance compared to angiosperms. This interpretation is supported by the angiosperm-dominated terpenoid biomarker composition found in detritic lignites from the same mines during a previous study (Bechtel et al., 2019). Low ββ/(ββ+αβ) hopane ratios and low sulfur contents imply freshwater conditions and bacterial activity under acidic pH during wood decomposition within topogenous mires. As indicated by different $\delta^{13}C$ values of ββ-C_{31} hopane (22R), slightly different microbial communities were involved in decomposition of OM of fossil wood and detritic lignite respectively.

Advanced cellulose decomposition removing preferentially the ^{13}C-enriched compounds from xylites is indicated to result in neglectable influence on $\delta^{13}C$ of cellulose, arguing for their applicability in environmental reconstructions. The significant differences in $\delta^{2}H$ between diterpenoids and *n*-alkanes, as well as between diterpenoids of different structural types are explained by differences in isotopic fractionation during lipid biosynthesis. The positive relationships between $\delta^{2}H$ and $\delta^{13}C$ of *n*-C_{29}, as well as between $\delta^{2}H$ of the C_{29} *n*-alkane and $\delta^{13}C$ of cellulose, imply variations in water availability and, thus, stomatal aperture, as the most probable cause for the obtained minor variations in isotopic composition of plant lipids and cellulose.

The results supplement the information obtained during our previous studies (Bechtel et al., 2007, 2019), as terpenoid biomarker composition in lignite is shown to be influenced by plant decomposition and differences in ecology between the habitats. Stable isotope data of cellulose and plant biomarkers of fossil wood are able to provide insights into environmental changes during peat accumulation.

Acknowledgements

This article is a contribution to the Research Project No. 2017/27/B/ST10/00001, funded by the National Science Centre, Poland. Critical remarks of two anonymous reviewers and Klaas Nierop (associate editor) are gratefully acknowledged. We thank Holger Wissel for the preparation of cellulose and the respective isotope analyses.

References

Arens, N.C., Jahren, A.H., Amundson, R., 2000. Can C3 plants faithfully record the carbon isotopic composition of atmospheric carbon dioxide? Paleobiology 261, 137–164.

Bechtel, A., Widera, M., Sachsenhofer, R.F., Gratzer, R., Lücke, A., Woszczyk, M., 2007. Biomarker and stable carbon isotope systematics of fossil wood from the second Lusatian lignite seam of the Lubstów deposit (Poland). Organic Geochemistry 38, 1850–1864.

Bechtel, A., Gratzer, R., Sachsenhofer, R.F., Gusterhuber, J., Lücke, A., Püttmann, W., 2008. Biomarker and carbon isotope variation in coal and fossil wood of Central Europe through the Cenozoic. Palaeogeography, Palaeoclimatology, Palaeoecology 262, 166–175.

Bechtel, A., Widera, M., Woszczyk, M., 2019. Composition of lipids from the First Lusatian lignite seam of the Konin Basin (Poland): Relationships with vegetation, climate and carbon cycling during the mid-Miocene Climatic Optimum. Organic Geochemistry 138, 103908.

Benner, R., Maccubbin, A.E., Hodson, R.E., 1984. Anaerobic biodegradation of the lignin and polysaccaride components of lignocellulose and synthetic lignin by sediment micro-flora. Applied and Environmental Microbiology 47, 998-1004.

Benner, R., Fogel, M.L., Sprague, E.K., Hodson, R.E., 1987. Depletion of ^{13}C in lignin and its implications for stable carbon isotope studies. Nature 329, 708–710.

Bottari, F., Marsili, A., Morelli, I., Pacchiani, M., 1972. Aliphatic and triterpenoid hydrocarbons from ferns. Phytochemistry 11, 2519–2523.

Bowen, G. J., 2008, Spatial analysis of the intra-annual variation of precipitation isotope ratios and its climatological corollaries, Journal of Geophysical Research, 113, D05113, doi:10.1029/2007JD009295.

Brassell, S.C., Comet, P.A., Eglinton, G., Isaacson, P.J., McEvoy, J., Maxwell, J.R., Thompson, I.D., Tibbetts, P.J.C., Volkman, J.K., 1980. The origin and fate of lipids in the Japan Trench. In: Douglas, A.G., Maxwell, J.R. (Eds.), Advances in Organic Geochemistry, 1979, Pergamon Press, Oxford, pp. 375–392.

Bruch, A.A., Uhl, D., Mosbrugger, V., 2007. Miocene climate in Europe-Patterns and evolution. A first synthesis of NECLIME. Palaeogeography, Palaeoclimatology, Palaeoecology 253, 1–7.

Casagrande, D.J., 1987. Sulphur in peat and coal. In: Scott, A.C. (ed.), Coal and Coal-Bearing Strata: Recent Advances. Geol. Soc. Spec. Publ., vol. 32. Geological Society, of London, pp. 87–105.

Chikaraishi, Y., Naraoka, H., Poulson, S.R., 2004. Carbon and hydrogen isotopic fractionation during lipid biosynthesis in a higher plant (Cryptomeria japonica). Phytochemistry 65, 323–330.

Chomiak, L., Wachocki, R., Maciaszek, P., Widera, M., Zieliński, T., 2019. Seismically-induced soft-sediment deformation in crevasse-splay microdelta deposits (Middle Miocene, central Poland). Geological Quarterly 63, 162–177.

Collister, J.W., Rieley, G., Stern, B., Eglinton, G., Fry, B., 1994. Compound-specific $\delta^{13}C$ analysis of leaf lipids from plants with differing carbon dioxide metabolism. OrganicGeochemistry 21, 619–627.

Cranwell, P.A., 1977. Organic geochemistry of Cam Loch (Sutherland) sediments. Chemical Geology 20, 205–221.

Diefendorf, A.F., Freimuth, E.J., 2017. Extracting the most from terrestrial plant-derived n-alkyl lipids and their carbon isotopes from the sedimentary record: A review. Organic Geochemistry 103, 1–21.

Diefendorf, A.F., Sberna, D.T., Taylor, D.W., 2015. Effect of thermal maturation on plant-derived terpenoids and leaf wax *n*-alkyl components. Organic Geochemistry 89–90, 61–70.

Diefendorf, A.F., Leslie, A.B., Wing, S.L., 2019. A phylogenetic analysis of conifer diterpenoids and their carbon isotopes for chemotaxonomic applications. Organic Geochemistry 127, 50–58.

Đoković, N., Mitrović, D., Životić, D., Bechtel, A., Sachsenhofer, R.F., Matić, V., Glamočanin, L., Stojanović, K., 2018. Petrographical and organic geochemical study of the lignite from the Smederevsko Pomoravlje field (Kostolac Basin, Serbia). International Jourmal of Coal Geology 195, 139–171.

Eglinton, G., Hamilton, R.J., 1967. Leaf epicuticular waxes. Science 156, 1322–1335.

Fabiańska, M., Kurkiewicz, S., 2013. Biomarkers, aromatic hydrocarbons and polar compounds in the Neogene lignites and gangue sediments of the Konin and Turoszów Brown Coal Basins (Poland). International Journal of Coal Geology 107, 24–44.

Feng, X., Epstein, S., 1995. Carbon isotopes in trees from arid environments and implications for reconstructing atmospheric CO_2 concentration. Geochim. Cosmochim. Acta 59, 2599–2608.

Fengel, D., Wegener, G., 1984. Wood Chemistry, Ultrastructure and Reactions, deGruyter, Berlin, pp. 217–220.

Ficken, K.J., Li, B., Swain, D.L., Eglinton, G., 2000. An *n*-alkane proxy for the sedimentary input of submerged/floating freshwater aquatic macrophytes. Organic Geochemistry 31, 745–749.

Freimuth, E.J., Diefendorf, A.F., Lowell, T.V., 2017. Hydrogen isotopes of *n*-alkanes and *n*-alkanoic acids as tracers of precipitation in a temperate forest and implications for paleorecords. Geochimica et Cosmochimica Acta 206, 166–183.

Grantham, P.J., Douglas, A.G., 1980. The nature and origin of sesquiterpenoids in some Tertiary fossil resins. Geochimica et Cosmochimica Acta 44, 1801–1810.

Hagemann, H.W., Hollerbach, A., 1979. Relationship between the macropetrographic and organic geochemical composition of lignites. In: Douglas, A.G., Maxwell, J.R. (Eds.), Advances in Organic Geochemistry. Pergamon Press, pp. 631–638.

Huang, Y., Lockheart, M.J., Collister, J.W., Eglinton, G., 1995. Molecular and isotopic biogeochemistry of the Miocene Clarkia Formation: hydrocarbons and alcohols. Organic Geochemistry 23, 785–801.

Inglis, G.N., Naafs B.D.A., Zeng, Y., McClymont, E.L., Evershed, R.P., Pancost, R.D., 2018. Distribution of geohopanoids in peat: Implications for the use of hopanoid-based proxies in natural archives. Geochimica et Cosmochimica Acta 224, 249–261.

Inglis, G.N., Naafs, D.A., Zheng, Y., Schellekens, J., Pancost, R.D., the T-GRES Peat Database collaboraters, 2019. $\delta^{13}C$ values of bacterial hopanoids and leaf waxes as tracers for methanotrophy in peatland. Geochimica et Cosmochimica Acta 260, 244–256.

Ivanov, D., Worobiec, E., 2017, Middle Miocene (Badenian) vegetation and climate dynamics in Bulgaria and Poland based on pollen data: Palaeogeography, Palaeoclimatology, Palaeoecology 467, 83–94.

Jahren, A.H., Sternberg, L.S.L., 2008. Annual patterns within tree rings of the Arctic middle Eocene (ca. 45 Ma): isotopic signatures of precipitation, relative humidity, and deciduousness. Geology 36, 99–102.

Kaneda, T., 1991. Iso- and anteiso-fatty acids in bacteria – biosynthesis, function, and taxonomic significance. Microbiological Reviews 55, 288–302.

Karrer, W., Cherbuliez, E., Eugster, C.H., 1977. Konstitution und Vorkommen der organischen Pflanzenstoffe. Ergänzungsband I., Birkhäuser, Basel, Stuttgart, 1038 pp.

Kasiński, J.R., Słodkowska, B., 2016. Factors controlling Cenozoic anthracogenesis in the Polish Lowlands. Geological Quarterly 60, 959–974.

Kwiecińska, B., Wagner, M., 1997. Classification of qualitative features of brown coal from Polish deposits according to petrographical, chemical and technological criteria. Wydawnictwo Centrum PPGSMiE Polskiej Akademii Nauk, Kraków, 35 pp. (in Polish with English summary).

Kwiecińska, B., Wagner, M., 2001. Application of Reflectance in Natural and Technological Classification of Brown Coal (Lignite). Wydawnictwo Akademii Górniczo-Hutniczej, Kraków, pp. 35. (in Polish).

LaFlamme, R.E., Hites, R.A., 1979. Tetra- and pentacyclic, naturally-occurring, aromatic hydrocarbons in recent sediments. Geochimica et Cosmochimica Acta 43, 1687–1691.

Lee, H., Feng, X., Mastalerz, M., Feakins, S.J., 2019. Characterizing lignin: Combining lignin phenol, methoxy quantification, and dual stable carbon and hydrogen isotopic techniques. Organic Geochemistry 136, 103894.

Liu, B., Zhao, C., Ma, J., Sun.Y., Püttmann, W., 2018. The origin of pale and dark layers in Pliocene lignite deposits from Yunnan Province, Southwest China, based on coal petrological and organic geochemical analyses. International Journal of Coal Geology 195, 172–188.

Logan, G.A., Eglinton, G., 1994. Biogeochemistry of the Miocene lacustrine deposit at Clarkia, northern Idaho, U.S.A. Organic Geochemistry 21, 857–870.

Lücke, A., Helle, G., Schleser, G.H., Figueiral, I., Mosbrugger, V., Jones, T.B., Rowe, N.P., 1999. Environmental history of German Lower Rhine Embayment during the Middle Miocene as reflected by carbon isotopes in brown coal. Palaeogeography, Palaeoclimatology, Palaeoecology 154, 339–352.

Marynowski, L., Otto, A., Zatoń, M., Philippe, M., Simoneit, B.R.T., 2007. Biomolecules preserved in 168 million year old fossil conifer wood. Naturwissenschaften 94, 228–236.

Matl K., Wagner M., 1985. Tuffogenic markers in Neogene sediments of Polish Lowlands and the Carpathian Foredeep. [In:] VIII Congress RCMNS, Symposium European Late Cenozoic Mineral Resources, Abstracts, Budapest, p. 367–369.

Merk, V., Chanana, M., Gaan, S., Burgert, I., 2016. Mineralization of wood by calcium carbonate insertion for improved flame retardancy. Holzforschung, 70, pp. 867-876.

Misra, M.K., Ragland, K.W., Baker, A.W., 1993. Wood ash composition as a function of furnace temperature. Biomass Bioenergy 4, 103-116.

Mitrović, D., Đoković, N., Životić, D., Bechtel, A., Šajnović, A., Stojanović, K., 2016. Petrographical and organic geochemical study of the Kovin lignite deposit, Serbia. International Journal of Coal Geology 168, 80–107.

Naafs, B.D.A., Inglis, G.N., Blewett, J., McClymont, E.L., Lauretano, V., Xie, S., Evershed, R.P., Pancost. R.D., 2019. The potential of biomarker proxies to trace climate, vegetation, and biogeochemical processes in peat: A review. Globalal and Planetary Change 179, 57–79.

Noble, R.A., Alexander, R., Kagi, R.I., Knox, J., 1985. Tetracyclic diterpenoid hydrocarbons in some Australian coals, sediments and crude oils. Geochimica et Cosmochimica Acta 49, 2141–2147.

O'Leary, M.H., 1981. Carbon isotopic fractionation in plants. Phytochemistry 20, 553–567.

Otto, A., Simoneit, B.R.T., 2002. Biomarkers of Holocene buried conifer logs from Bella Coola and north Vancouver, British Columbia, Canada. Organic Geochemistry 33, 1241–1251.

Otto, A., Wilde, V., 2001. Sesqui-, di-, and triterpenoids as chemosystematic markers in extant conifers – a review. Botanical Review 67, 141–238.

Otto, A., Walther, H., Püttmann, W., 1997. Sesqui- and diterpenoid biomarkers in *Taxodium*-rich Oligocene oxbow lake clays, Weisselster basin, Germany. Organic Geochemistry 26, 105–115.

Ourisson, G., Albrecht, P., Rohmer, M., 1979. The hopanoids: palaeo-chemistry and biochemistry of a group of natural products. Pure and Applied Chemistry 51, 709–729.

Pancost, R.D., van Geel, B., Baas, M., Sinninge Damsté, J.S., 2000. $\delta^{13}C$ values and radiocarbon dates of microbial biomarkers as tracers for carbon recycling in peat deposits. Geology 28, 663–666.

Pancost, R.D., Steart, D.S., Handley, L., Collinson, M.E., Hooker, J.J., Scott, A.C., Grassineau, N.V., Glasspool, I.J., 2007. Increased terrestrial methane cycling at the Palaeocene–Eocene thermal maximum. Nature 449, 332–335.

Pettersen, R.C. (1984). The chemical composition of wood. In: Roswell, R.M. (Ed.), The chemistry of solid wood, Washington D.C., American Chemical Society, pp. 57–126.

Philp, R.P., 1985. Fossil fuel biomarkers. Applications and spectra. Methods in Geochemistry and Geophysics 23, 1–294.

Piwocki, M., 1987. Chemical and technological properties of the main groups of Tertiary brown coal seams in Poland. Biuletyn Instytutu Geologicznego 357, 41–60 (in Polish with English summary).

Piwocki, M., Ziembińska-Tworzydło, M., 1997. Neogene of the Polish Lowlands — lithostratigraphy and pollen-spore zones. Geological Quarterly 41, 21–40.

Poole, I., Dolezych, M., Kool, J., van der Burgh, J., van Bergen, P.F., 2006. Do stable carbon isotopes of brown coal woods record changes in Lower Miocene palaeoecology? Palaeogeography, Palaeoclimatology, Palaeoecology 236, 345–354.

Püttmann, W., Bracke, R., 1995. Extractable organic compounds in the clay mineral sealing of a waste disposal site. Organic Geochemistry 23, 43–54.

Rohmer, M., Bisseret, P., 1994. Hopanoid and other polyterpenoid biosynthesis in eubacteria. ACS Symposium Series 562, 31–43.

Rohmer, M., Bisseret, P., Neunlist, S., 1992. The hopanoids, prokaryotic triterpenoids and precursors of ubiquitous molecular fossils. In: Moldowan, J.M., Albrecht, P., Philp, R.P. (Eds.), Biological Markers in Sediments and Petroleum, Prentice Hall, Englewood Cliffs, N.J., pp. 1–17.

Rullkötter, J., Peakman, T.M., ten Haven, H.L., 1994. Early diagenesis of terrigenous triterpenoids and its implications for petroleum geochemistry. Organic Geochemistry 21, 215–233.

Sachse, D., Radke, J., Gleixner, G., 2004. Hydrogen isotope ratios of recent lacustrine sedimentary *n*-alkanes record modern climate variability. Geochimica et Cosmochimica Acta 68, 4877–4889.

Sachse, D., Radke, J., Gleixner, G., 2006. δD values of individual *n*-alkanes from terrestrial plants along a climatic gradient – Implications for the sedimentary biomarker record. Organic Geochemistry 37, 469–483.

Sachse, D., Billault I., Bowen, G.J., Chikaraishi, Y., Dawson, T.E., Feakins, S.J., Freeman, K.H., Magill, C.R., McInerney, F.A., van der Meer, M.T.J., Polissar, P., Robins, R.J., Sachs, J.P., Schmidt, H.-L., Sessions, A.L., White, J.W.C., West, J.B., Kahmen, A., 2012. Molecular Paleohydrology: Interpreting the hydrogen-isotopic composition of lipid biomarkers from Photosynthesizing Organisms. Annual Review of Earth and Planetary Sciences 40, 221–249.

Sadowska, A., Giża, B., 1991. The flora and age of the brown coal from Pątnów. Acta Palaeobotanica 31, 201–214.

Schimmelmann, A., Sessions, A.L., Mastalerz, M, 2006. Hydrogen isotopic (D/H) composition of organic matter during diagenesis and thermal maturation. Annual Review of Earth and Planetary Sciences 34, 501–533.

Schleser, G.H., 1995. Parameters determining carbon isotope ratios in plants. In: Frenzel, B. (ed.), Problems of Stable Isotopes in Tree-Rings, Lake Sediments and Peat-Bogs as Climatic Evidence for the Holocene. European Science Foundation Special Issue 15, pp. 71–96.

Schleser, G.H., Frielingsdorf, J., Blair, A., 1999. Carbon isotope behaviour in wood and cellulose during artificial aging. Chemical Geology 158, 121–130.

Sessions, A.L., Burgoyne, T.W., Schimmelmann, A., Hayes, J.M., 1999. Fractination of hydrogen isotopes in lipid biosynthesis. Organic Geochemistry 30, 1193–1200.

Simoneit, B.R.T., Mazurek, M.A., 1982. Organic matter of the troposphere – II. Natural background of biogenic lipid matter in aerosols over the rural western United States. Atmospheric Environment 16, 2139–2159.

Spyckerelle, C., Greiner, A.C., Albrecht, P., Ourisson, G., 1977. Aromatic hydrocarbons from geological sources. Part III. Journal of Chemical Research (M), 3746–3777.

Stefanova, M., Oros, D.R., Otto, A., Simoneit, B.R.T., 2002. Polar aromatic biomarkers in the Miocene Maritza-East lignite, Bulgaria. Organic Geochemistry 33, 1079–1091.

Sukh Dev, 1989. Terpenoids. In: Rowe, J.W. (ed.), Natural Products of Woody Plants, Vol. 1, pp. 691–807, Springer, Berlin.

ten Haven, H.L., Peakman, T.M., Rullkötter, J., 1992. Early diagenetic transformation of higher-plant triterpenoids in deep-sea sediments from Baffin Bay. Geochimica et Cosmochimica Acta 56, 2001–2024.

Tipple, B.J., Meyers, S.R., Pagani, M., 2010. Carbon isotope ratio of Cenozoic CO_2: a comparative evaluation of available geochemical proxies. Paleoceanography 25, PA3202

Tuo, J., Wang, X., Chen, J., Simoneit, B.R.T., 2003. Aliphatic and diterpenoid hydrocarbons and their individual carbon isotope compositions in coals from the Liaohe Basin, China. Organic Geochemistry 34, 1615–1625.

Tuo, J., Zhang, M., Wang, X., Zhang, C., 2006. Hydrogen isotope ratios of aliphatic and diterpenoid hydrocarbons in coals and carbonaceous mudstones from the Liaohe Basin, China. Organic Geochemistry 37, 165–176.

van Bergen, P.F., Poole, I., 2002. Stable carbon isotopes of wood: a clue to palaeoclimate? Palaeogeography, Palaeoclimatology, Palaeoecology 182, 31–45.

Volkman, J.K., 1986. A review of sterol markers for marine and terrigenous organic matter. Organic Geochemistry 9, 83–99.

Volkman, J.K., Johns, R.B., Gillan, F.T., Perry, G.J., 1980. Microbial lipids of an intertidal sediment – I. Fatty acids and hydrocarbons. Geochimica et Cosmochimica Acta 44, 1113–1143.

Wagner M., 1984. Clay kaolinite (paratonstein) rocks from the Bełchatów brown coal deposit (in Polish with English summary). Kwartalnik Geologiczny 25, 111–120.

Wakeham, S.G., Schaffner, C., Giger, W., 1980. Polycyclic aromatic hydrocarbons in Recent lake sediments. II. Compounds derived from biological precursors during early diagenesis. Geochimimica et Cosmochimica Acta 44, 415–429.

Widera, M., 2010. The morphology of fossil pebbles as a tool for determining their transport processes (Koźmin South lignite open-cast pit, central Poland). Annales Societatis Geologorum Poloniae 80, 315–325.

Widera, M., 2013. Changes of the lignite seam architecture – a case study from Polish lignite deposits. International Journal of Coal Geology 114, 60–73.

Widera, M., 2016. Depositional environments of overbank sedimentation in the lignite-bearing Grey Clays Member: New evidence from Middle Miocene deposits of central Poland. Sedimentary Geology 335, 150–165.

Widera, M., Chomiak, L., Zieliński, T., 2019. Sedimentary facies, processes and paleochannel pattern of an anastomosing river system: an example from the Upper Neogene of Central Poland. Journal of Sedimentary Research 89, 487–507.

Wissel, H., Mayr, C., Lücke, A., 2008. A new approach fort he isolation of cellulose from aquatic plant tissue and freshwater sediments for stable isotope analysis. Organic Geochemistry 39, 1545–1561.

Wolff, G.A., Trendel, J.M., Albrecht, P., 1989. Novel monoaromatic triterpenoid hydrocarbons occuring in sediments. Tetrahedron 45, 6721–6728.

Worobiec, E., Widera, M., Worobiec, G., Kurdziel, B., 2020. Middle Miocene palynoflora from the Adamów lignite deposit, central Poland. Palynology, doi: 10.1080/01916122.2019.1697388

Yang, H., Huang, Y., 2003. Preservation of lipid hydrogen isotope ratios in Miocene lacustrine sediments and plant fossils at clarkia, northern Idaho, USA. Organic Geochemistry 34, 431–423.

Zachos, J., Pagani, M., Sloan, L., Thomas, E., Billups, K., 2001. Trends, rhythms, and aberrations in global climate 65 Ma to present. Science 292, 686–693.

Captions of Figures

Fig. 1: (a) Location of the studied lignite opencast mines in the Konin Basin (Poland); and lignite lithotypes, structural elements, and position of xylite samples in the profiles from the (b) Adamów, (c) Jóźwin IIB, and (d) Tomisławice opencast mines.

Fig. 2: Representative photomicrographs of wood fragments (reflected light; oil immersion): (a) Textinite in ungelified sample AX-01, (b) same field as in (a) (blue light irradiation), (c) textinite/textoulminite with a phlobaphinite (P) in weakly gelified sample TX-10, (d) same filed as in (c) (blue light irradiation), (e) textoulminite/ulminite in sample JX-3 showing advanced gelification, (f) same field as in (c) (blue light irradiation).

Fig. 3: Sampling position and variation of concentrations and concentration ratios of lipids within the xylites from the First Lusatian lignite seam at the Adamów, the Jóźwin IIB, and the Tomisławice mines.

Fig. 4: Cross-correlation between extractable organic matter (EOM) and cellulose yields.

Fig. 5: Total ion current chromatograms of the (a) hydrocarbon fraction, (b) the ketone fraction, (c) the alcohol fraction, and (d) the carboxylic acids obtained from the xylite sample AX-09, Std. = Internal Standard (squalane (F1), 1,1´-binaphthyl (F2), 1-nonadecanol (F3), nonadecanoic acid (FA), respectively).

Fig. 6: Depth trends of carbon isotopic compositions of (a) TOC and cellulose , (b) C_{27}, C_{29}, and C_{31} *n*-alkanes, and (c) diterpenoids, and of hydrogen isotopic compositions of (d) C_{27}, C_{29}, and C_{31} *n*-alkanes, and (e) diterpenoids within the studied profiles from the Adamów, Jóźwin IIB, and Tomisławice mines.

Fig. 7: Relative abundances of terpenoid biomarkers in the lipid fractions of the xylites.

Fig. 8: Cross-correlation between the di-/(di- + tri-)terpenoids ratios and ash yields.

Fig. 9: Relationship between the concentrations of hopanoids and the cellulose yields of the xylites.

Fig. 10: Correlations of (a) $\delta^{13}C$ of cellulose and TOC of xylites, respectively, versus cellulose yields, and of (b) carbon isotope differences between cellulose and TOC of xylites versus cellulose yields.

Fig. 11: Relationships between (a) $\delta^{13}C$ and $\delta^{2}H$ of the C_{29} *n*-alkanes, and between (b) $\delta^{13}C$ of cellulose and $\delta^{2}H$ of *n*-C_{29}.

Research Highlights

- Xylites are affected by weak gelification and advanced cellulose decomposition
- $\delta^{13}C$ of xylites reflect the extent of cellulose decomposition
- Xylites represent wood remains of the same species of conifers in the lignite
- Fluctuating $\delta^{13}C$ and $\delta^{2}H$ of lipids within the seam are caused by water availability

Table 1: Sample locations, maceral variety and fluorescence of telohuminite, bulk geochemical parameters, and extractable organic matter yields

Deposit	Sample	Altitude (m a.s.l.)[e]	Maceral variety	Fluorescence intensity	Ash	TOC[a]	TIC[b]	S[c]	$\delta^{13}C$ TOC	$\delta^{13}C$ Cellulose	Cellulose yield	EOM[d]
					(wt%)[f]				(‰, VPDB)		(wt%)	(mg/g TOC)
Adamów	AX-01	61.7	Textinite	High	3.2	38.4	3.5	0.28	-25.3	-21.6	6.8	46.2
Adamów	AX-02	62.3			2.8	41.0	2.7	0.32	-24.7	-20.9	6.2	39.9
Adamów	AX-03	63.0	Textinite	High	4.1	39.3	2.4	0.27	-24.0	-19.9	6.3	54.4
Adamów	AX-04	63.8			2.6	41.8	3.0	0.29	-24.6	-21.3	15.0	19.3
Adamów	AX-05	64.3	Textinite	High	3.0	42.7	0.5	0.26	-25.6	-21.9	10.6	29.0
Adamów	AX-06	64.7			3.5	40.5	2.1	0.30	-25.2	-21.7	7.4	61.5
Adamów	AX-07	65.5	Textinite/textoul.[g]	High/moderate	9.5	37.9	3.8	1.80	-26.2	-22.5	5.8	59.4
Adamów	AX-08	66.1			4.1	34.0	0.7	4.28	-24.9	-21.9	13.3	26.4
Adamów	AX-09	66.8			7.7	45.0	2.0	1.60	-26.0	-22.1	5.9	47.3
Adamów	AX-10	67.6			2.4	43.6	2.0	0.36	-26.1	-22.7	9.1	35.0
Jóźwin IIB	JX-01	41.5			11.0	41.5	2.5	1.57	-24.4	-21.4	5.7	42.8
Jóźwin IIB	JX-02	42.3			8.4	36.9	3.3	1.38	-26.6	-22.4	1.6	58.9
Jóźwin IIB	JX-03	43.2	Textoul./ulminite	Moderate/weak	2.7	52.8	n.d.[h]	1.44	-24.3	-22.0	18.2	21.8
Jóźwin IIB	JX-04	44.3			6.2	43.1	3.5	1.49	-25.4	-21.0	4.8	64.6
Jóźwin IIB	JX-05	44.8	Textoul.	Moderate/weak	4.1	44.8	3.8	2.06	-25.5	-21.5	5.2	39.9
Jóźwin IIB	JX-06	45.9			9.9	48.2	0.4	4.10	-25.5	-21.5	3.7	38.3
Jóźwin IIB	JX-07	46.1	Textoul.	Moderate	5.6	43.8	3.0	3.22	-25.5	-21.9	3.7	52.9
Tomisławice	TX-01	53.1			17.6	32.5	2.8	2.54	-24.6	-20.4	5.9	35.6
Tomisławice	TX-02	54.2	Textinite/textoul.	High/moderate	2.7	53.6	n.d.	0.35	-24.6	-21.9	21.8	26.4
Tomisławice	TX-03	55.0			3.0	53.2	n.d.	0.33	-24.4	-20.9	16.2	29.9
Tomisławice	TX-04	56.2			3.9	48.7	n.d.	0.30	-24.9	-20.6	7.4	43.6
Tomisławice	TX-05	57.3			5.5	45.9	2.5	0.26	-26.1	-21.9	4.1	49.6
Tomisławice	TX-06	58.2	Textinite	High	3.8	47.9	n.d.	0.36	-23.8	-20.3	24.2	18.3
Tomisławice	TX-07	59.2			3.7	48.8	0.7	0.57	-23.8	-20.6	19.4	20.1
Tomisławice	TX-08	60.4	Textinite	High	3.9	45.7	n.d.	0.60	-23.8	-20.2	13.5	35.6
Tomisławice	TX-09	61.3			4.1	45.2	n.d.	0.76	-25.3	-22.1	18.1	29.0
Tomisławice	TX-10	62.0	Textinite/textoul.	High/moderate	4.2	46.5	n.d.	1.23	-23.7	-20.6	19.3	23.8

[a] Total organic carbon, [b] Total inorganic carbon content, [c] Total sulphur content, [d] Extractable organic matter, [e] Meter above sea level, [f] Weight percent, [g] Textoulminite, [h] not detectable

Table 2: Proportions of hydrocarbons + ketones, carboxylic acids, alcohols, and macromolecular substances (i.e. resins) relative to EOM, and concentrations and concentration ratios of compounds and compound groups within the EOM of lignite samples

Deposit	Sample	HCs[a] + Ketones	Acids	Alcohols	Resins	*n*-Alkanes	Steroids	Hopanoids	Diter-penoids	Triter-[b] penoids	ββ/(ββ + αβ) C_{31} Hopanes	Di-/(Di- + Tri-) terpenoids[c]
		(wt%, EOM)				(μg/g TOC)						
Adamów	AX-01	15.8	15.2	17.0	52	94	373	67	1698	17	0.06	0.99
Adamów	AX-02	11.9	10.8	14.7	63	102	159	69	630	65	0.08	0.91
Adamów	AX-03	11.3	9.4	12.3	67	243	344	84	741	36	0.07	0.95
Adamów	AX-04	9.6	13.2	10.5	67	144	190	41	281	24	0.06	0.92
Adamów	AX-05	8.5	11.9	14.6	65	125	222	55	153	19	0.12	0.89
Adamów	AX-06	11.7	8.3	9.2	71	262	120	74	917	45	0.07	0.95
Adamów	AX-07	10.9	6.5	11.1	71	440	53	108	466	84	0.07	0.85
Adamów	AX-08	8.4	12.1	15.7	64	75	209	73	235	30	0.06	0.89
Adamów	AX-09	14.4	18.7	20.3	47	383	298	66	1468	201	0.08	0.88
Adamów	AX-10	9.8	10.4	17.9	62	250	137	84	329	32	0.10	0.91
Jóźwin IIB	JX-01	5.1	12.4	22.3	60	258	47	69	148	47	0.09	0.76
Jóźwin IIB	JX-02	4.6	7.6	18.4	69	298	84	147	553	74	0.07	0.88
Jóźwin IIB	JX-03	9.9	9.1	14.5	67	93	104	45	948	56	0.06	0.94
Jóźwin IIB	JX-04	7.7	12.0	15.1	65	263	209	159	640	121	0.11	0.84
Jóźwin IIB	JX-05	5.3	7.7	10.8	76	85	367	133	513	86	0.09	0.86
Jóźwin IIB	JX-06	4.2	11.3	17.9	67	234	245	120	281	81	0.14	0.78
Jóźwin IIB	JX-07	6.9	13.8	16.7	63	76	127	85	596	53	0.11	0.92
Tomisławice	TX-01	5.0	10.4	9.3	75	232	104	69	169	58	0.22	0.74
Tomisławice	TX-02	5.3	13.5	15.2	66	221	191	42	331	49	0.13	0.87
Tomisławice	TX-03	4.9	7.9	21.1	66	289	176	56	622	82	0.16	0.88
Tomisławice	TX-04	7.6	8.5	13.5	70	99	262	75	765	95	0.15	0.89
Tomisławice	TX-05	9.0	6.6	10.8	74	166	74	95	481	90	0.13	0.84
Tomisławice	TX-06	6.2	10.9	16.6	66	218	230	63	623	106	0.16	0.85
Tomisławice	TX-07	7.3	9.2	19.2	64	176	111	56	462	49	0.12	0.90
Tomisławice	TX-08	9.2	10.7	22.3	58	82	113	84	227	36	0.13	0.86
Tomisławice	TX-09	8.4	7.6	20.7	63	77	106	74	338	42	0.14	0.89
Tomisławice	TX-10	6.9	8.9	17.6	67	22	117	37	297	22	0.09	0.93

[a] Hydrocarbons, [b] Angiosperm-derived triterpenoids, [c] Ratios of diterpenoids to the sum of di- plus triterpenoids

Table 3: Carbon isotopic composition of plant lipids and hopanoids

Deposit	Sample	*n*-C_{27}	*n*-C_{29}	*n*-C_{31}	Nor-abietane	Pimarane	α-Phyllo-cladane	αβ-C_{31} Hopane (22R)	ββ-C_{31} Hopane	Hop-17(21)-ene
		$\delta^{13}C$ (‰, VPDB)								
Adamów	AX-01	-29.8	-30.6	-30.9	-24.9	n.d.	n.d.	-26.6	n.d.	n.d.
Adamów	AX-02	-30.0	-30.3	-30.5	n.d.	n.d.	-25.2	-27.2	n.d.	n.d.
Adamów	AX-03	-29.1	-29.6	n.d.	n.d.	-26.2	-24.8	-27.9	n.d.	n.d.
Adamów	AX-04	-29.9	-30.2	-30.0	n.d.	n.d.	-25.4	-26.8	n.d.	n.d.
Adamów	AX-05	-30.6	-30.9	-30.5	n.d.	n.d.	-25.7	-25.6	n.d.	n.d.
Adamów	AX-06	-29.6	-29.9	n.d.	-24.8	n.d.	-25.4	-26.5	n.d.	n.d.
Adamów	AX-07	-30.5	-31.3	-30.8	-24.8	-26.3	-25.5	-27.4	n.d.	n.d.
Adamów	AX-08	-30.0	-30.6	-29.8	n.d.	-26.3	-25.1	-25.8	n.d.	-34.2
Adamów	AX-09	-30.6	-31.0	-30.9	-25.1	-26.5	-25.6	-26.5	n.d.	-30.7
Adamów	AX-10	-29.8	-30.9	-30.7	n.d.	n.d.	-25.3	-26.4	n.d.	n.d.
Jóźwin IIB	JX-01	-30.5	-30.8	-30.8	-24.5	-25.8	-25.1	-25.6	-27.9	-32.3
Jóźwin IIB	JX-02	-30.9	-31.4	-31.1	n.d.	-26.3	-25.7	-26.2	-28.6	-34.2
Jóźwin IIB	JX-03	n.d.[a]	n.d.	n.d.	-24.9	-25.9	-25.2	-25.7	n.d.	n.d.
Jóźwin IIB	JX-04	-30.7	-31.1	-30.8	-25.0	-26.1	-25.4	-26.1	-27.5	-31.5
Jóźwin IIB	JX-05	n.d.	n.d.	n.d.	-24.8	n.d.	n.d.	-25.8	-26.9	-29.5
Jóźwin IIB	JX-06	-29.7	-30.4	-30.9	-24.7	-26.2	-25.3	-26.2	-28.3	-30.7
Jóźwin IIB	JX-07	n.d.	n.d.	n.d.	-24.6	-25.8	n.d.	-25.7	n.d.	-33.9
Tomisławice	TX-01	-29.6	-30.1	-30.5	n.d.	-25.9	-25.2	-26.1	n.d.	n.d.
Tomisławice	TX-02	-30.7	-31.2	-30.8	-25.1	-26.4	-25.4	-25.6	-26.9	-34.4
Tomisławice	TX-03	-30.1	-30.2	-30.4	-24.7	-26.0	-25.1	-26.3	-27.3	-33.6
Tomisławice	TX-04	-29.8	-30.1	n.d.	-24.6	n.d.	-25.2	-25.7	-27.4	n.d.
Tomisławice	TX-05	-30.9	-31.5	-31.2	-24.7	-25.9	-25.3	-26.4	n.d.	-29.3
Tomisławice	TX-06	-30.2	-30.0	-30.5	-24.4	-25.7	-25.0	-25.8	-26.6	-33.1
Tomisławice	TX-07	-30.5	-30.6	-30.5	-24.7	-26.0	-25.4	-26.0	-27.1	-31.7
Tomisławice	TX-08	-29.7	-30.5	-30.4	-24.5	n.d.	-25.1	-25.6	-26.9	-32.8
Tomisławice	TX-09	-30.6	-31.4	-30.7	-24.7	-26.1	-25.5	-26.1	-27.2	-30.3
Tomisławice	TX-10	n.d.	n.d.	n.d.	-24.2	-25.9	-25.3	-26.6	-27.4	-32.7

[a] not detectable due to low peak intensities

Table 4: Hydrogen isotopic composition of plant lipids and hopanoids

Deposit	Sample	*n*-C_{27}	*n*-C_{29}	*n*-C_{31}	Nor-abietane	Pimarane	α-Phyllo-cladane	αβ-C_{31} Hopane (22R)	Hop-17(21)-ene
		δ^2H (‰, VSMOW)							
Adamów	AX-01	-170	-172	-174	-241	n.d.	n.d.	-153	n.d.
Adamów	AX-02	-168	-171	n.d.	n.d.	n.d.	-236	-156	n.d.
Adamów	AX-03	-172	-167	n.d.	n.d.	-275	-231	-157	n.d.
Adamów	AX-04	-166	-170	n.d.	n.d.	n.d.	-244	-154	n.d.
Adamów	AX-05	-171	-169	-173	n.d.	n.d.	n.d.	-147	n.d.
Adamów	AX-06	-169	-170	n.d.	-244	n.d.	-233	-159	n.d.
Adamów	AX-07	-173	-174	n.d.	-249	-289	-241	-154	n.d.
Adamów	AX-08	-169	-171	n.d.	n.d.	-282	n.d.	-160	-212
Adamów	AX-09	-168	-173	-169	-256	-290	-238	-145	-206
Adamów	AX-10	-168	-172	n.d.	n.d.	n.d.	-240	-161	n.d.
Jóźwin IIB	JX-01	-165	-169	-172	-259	-279	n.d.	-160	-230
Jóźwin IIB	JX-02	-169	-173	-173	n.d.	-289	-252	-146	-224
Jóźwin IIB	JX-03	n.d.[a]	n.d.	n.d.	-251	-279	-242	-159	n.d.
Jóźwin IIB	JX-04	-168	-171	n.d.	n.d.	-282	-248	-170	-209
Jóźwin IIB	JX-05	n.d.	n.d.	n.d.	-255	n.d.	n.d.	-160	-232
Jóźwin IIB	JX-06	-167	-168	-172	-246	-283	-236	-157	-198
Jóźwin IIB	JX-07	n.d.	n.d.	n.d	n.d.	-275	n.d.	-174	-202
Tomisławice	TX-01	-162	-167	n.d	n.d.	-276	-246	-151	n.d.
Tomisławice	TX-02	-168	-172	-174	-251	-290	-251	-175	-224
Tomisławice	TX-03	-167	-168	-172	n.d.	-275	-244	-167	-203
Tomisławice	TX-04	-167	-168	-173	-264	n.d.	-247	-162	n.d.
Tomisławice	TX-05	-170	-172	n.d	n.d.	-294	-252	-181	-227
Tomisławice	TX-06	-166	-167	n.d	n.d.	-286	n.d.	-159	-206
Tomisławice	TX-07	-168	-171	n.d	-257	-289	-245	-167	-199
Tomisławice	TX-08	-168	-169	n.d	-253	n.d.	-237	-159	-222
Tomisławice	TX-09	-166	-170	-172	-248	-279	-238	-143	-211
Tomisławice	TX-10	n.d.	n.d.	n.d.	-253	-282	n.d.	-157	-229

[a] not detectable due to low peak intensities

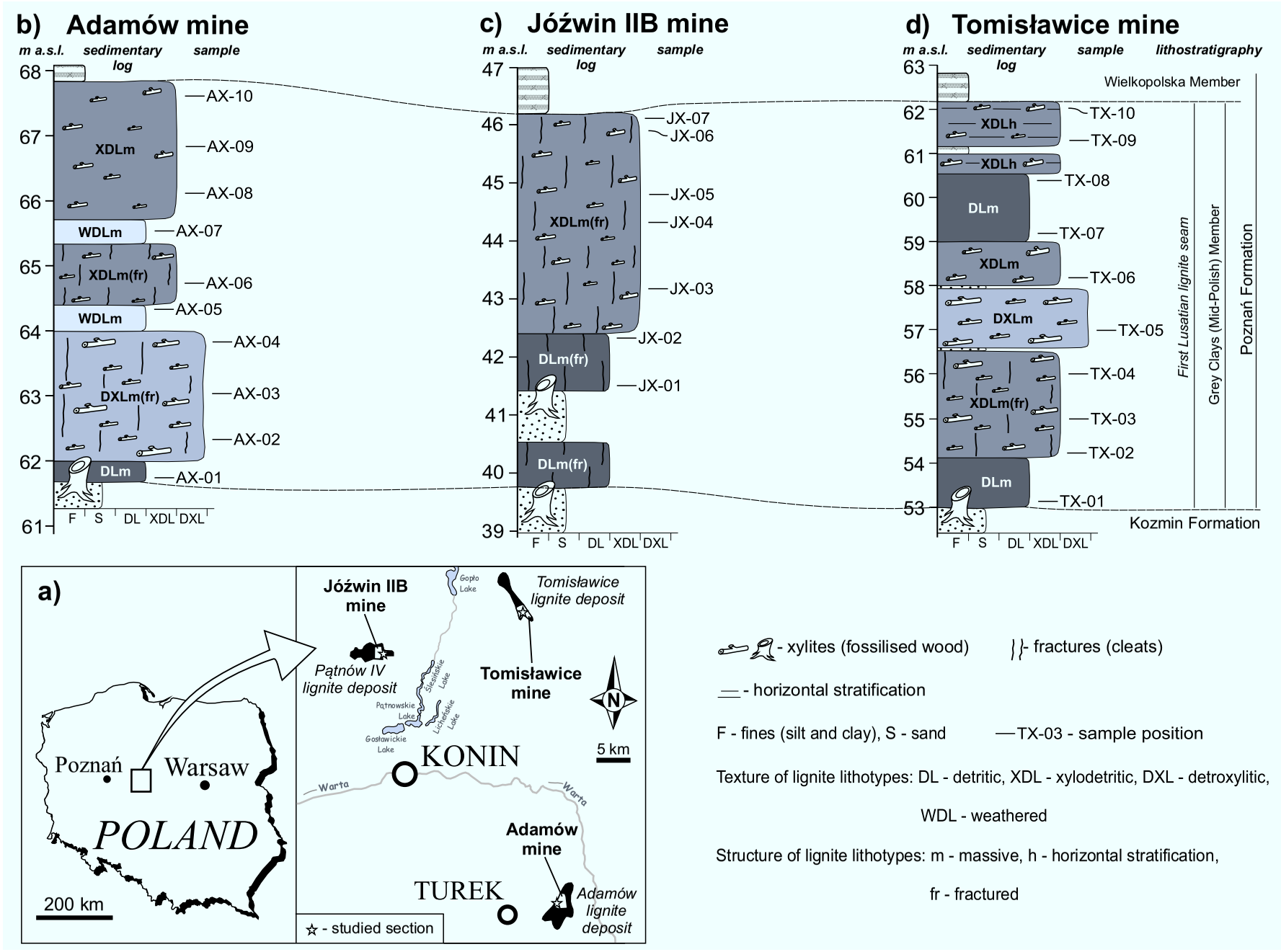
b) Adamów mine
m a.s.l.
sedimentary log
sample
68
67
66
65
64
63
62
61
XDLm
WDLm
XDLm(fr)
WDLm
DXLm(fr)
DLm
AX-10
AX-09
AX-08
AX-07
AX-06
AX-05
AX-04
AX-03
AX-02
AX-01
F S DL XDL DXL
c) Jóźwin IIB mine
m a.s.l.
sedimentary log
sample
47
46
45
44
43
42
41
40
39
XDLm(fr)
DLm(fr)
DLm(fr)
JX-07
JX-06
JX-05
JX-04
JX-03
JX-02
JX-01
F S DL XDL DXL
d) Tomisławice mine
m a.s.l.
sedimentary log
sample
lithostratigraphy
63
62
61
60
59
58
57
56
55
54
53
Wielkopolska Member
XDLh
XDLh
DLm
XDLm
DXLm
XDLm(fr)
DLm
TX-10
TX-09
TX-08
TX-07
TX-06
TX-05
TX-04
TX-03
TX-02
TX-01
Kozmin Formation
First Lusatian lignite seam
Grey Clays (Mid-Polish) Member
Poznań Formation
F S DL XDL DXL
a)
Poznań
Warsaw
POLAND
200 km
Jóźwin IIB mine
Pątnów IV lignite deposit
Tomisławice lignite deposit
Tomisławice mine
Gopło Lake
Pątnowskie Lake
Gosławickie Lake
Ślesińskie Lake
Licheńskie Lake
KONIN
Warta
Warta
N
5 km
Adamów mine
TUREK
Adamów lignite deposit
☆ - studied section
- xylites (fossilised wood)
- fractures (cleats)
- horizontal stratification
F - fines (silt and clay), S - sand
TX-03 - sample position
Texture of lignite lithotypes: DL - detritic, XDL - xylodetritic, DXL - detroxylitic, WDL - weathered
Structure of lignite lithotypes: m - massive, h - horizontal stratification, fr - fractured

Fig. 1

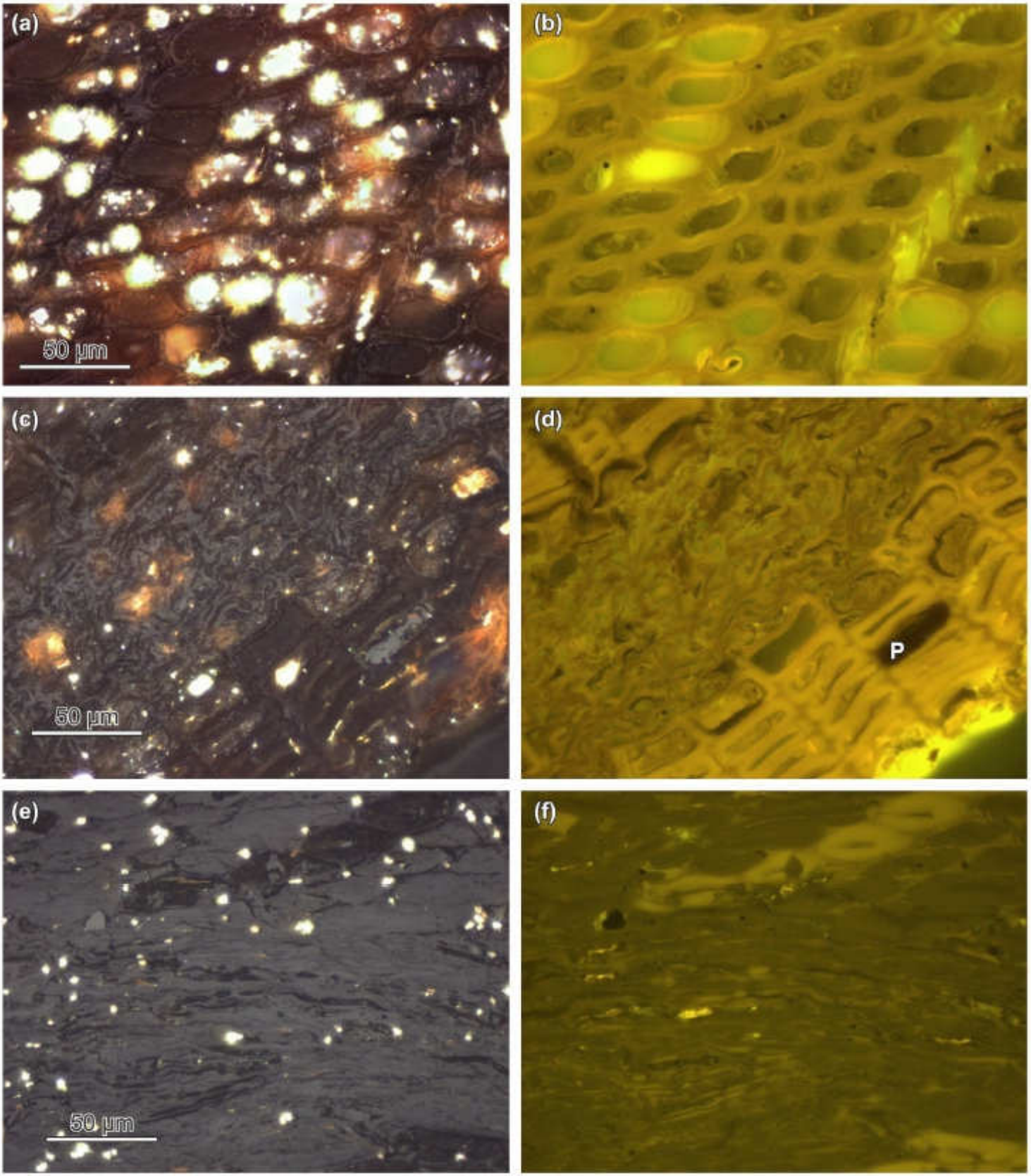

Fig. 2

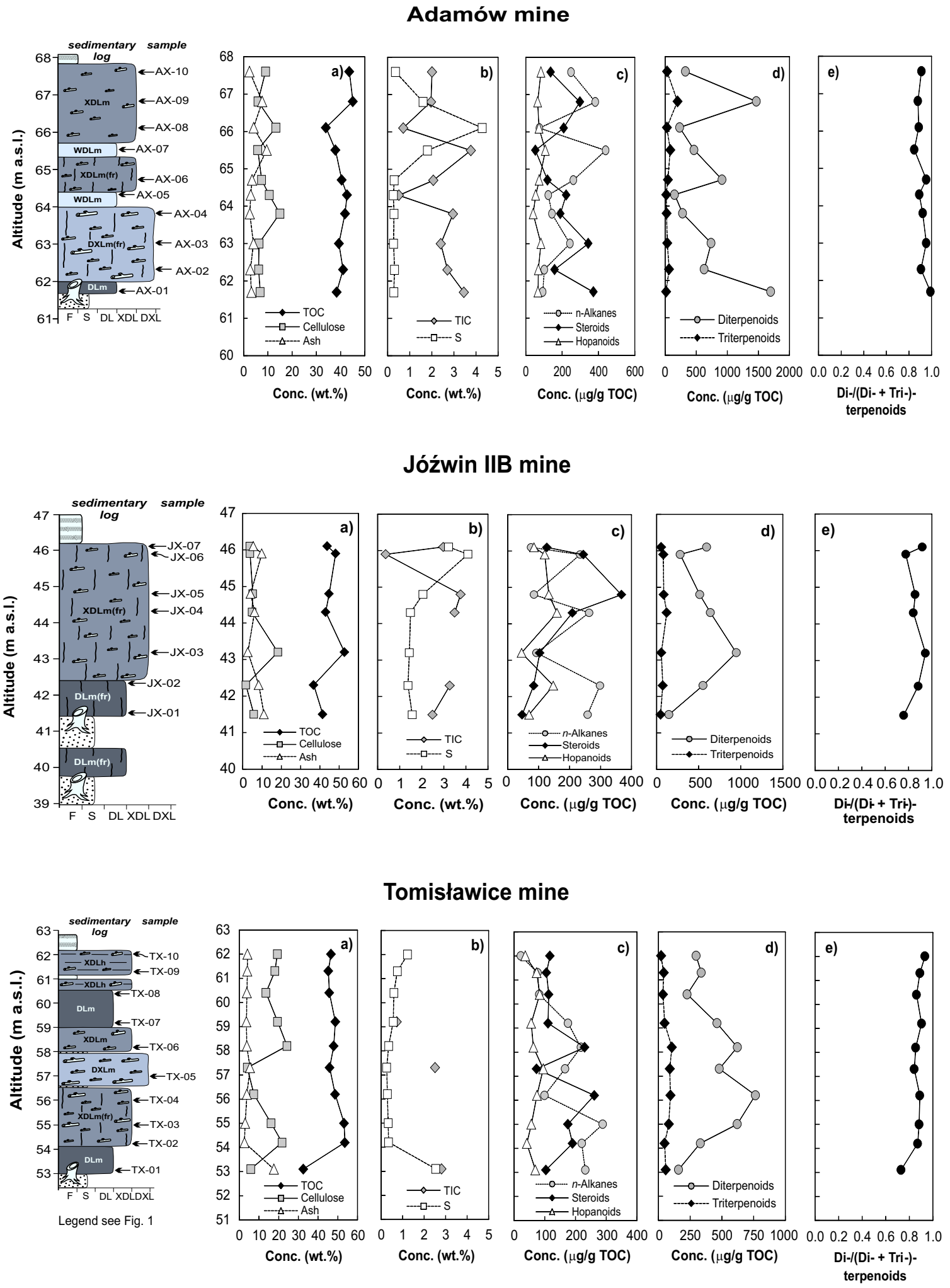
Adamów mine
sedimentary log
sample
Altitude (m a.s.l.)
XDLm
WDLm
XDLm(fr)
DXLm(fr)
DLm
AX-10
AX-09
AX-08
AX-07
AX-06
AX-05
AX-04
AX-03
AX-02
AX-01
F S DL XDL DXL
a)
b)
c)
d)
e)
TOC
Cellulose
Ash
TIC
S
n-Alkanes
Steroids
Hopanoids
Diterpenoids
Triterpenoids
Conc. (wt.%)
Conc. (µg/g TOC)
Di-/(Di- + Tri-)-terpenoids
Jóźwin IIB mine
JX-07
JX-06
JX-05
JX-04
JX-03
JX-02
JX-01
DLm(fr)
n-Alkanes
Tomisławice mine
XDLh
TX-10
TX-09
TX-08
TX-07
TX-06
TX-05
TX-04
TX-03
TX-02
TX-01
Legend see Fig. 1

Fig. 3

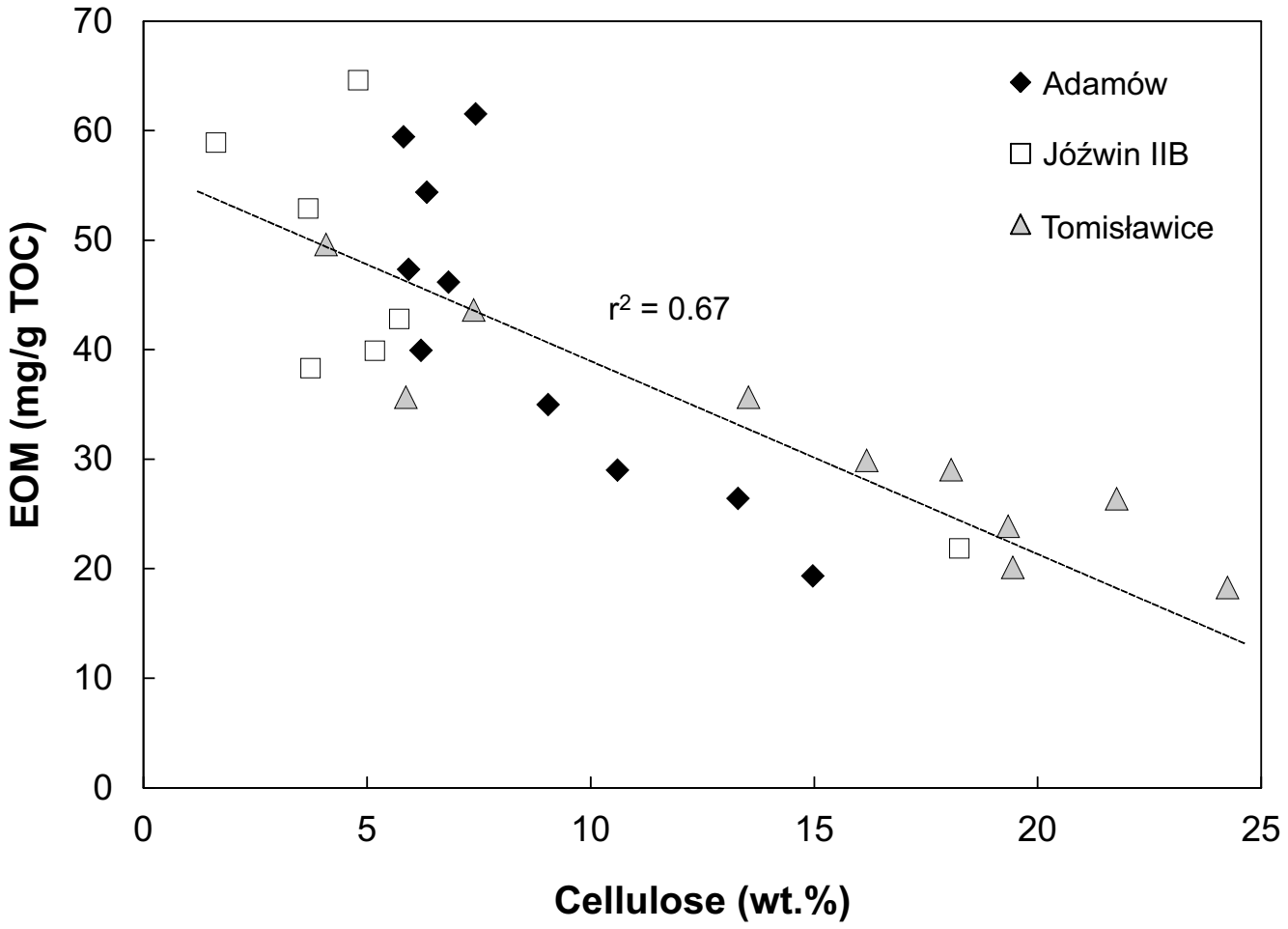
70
60
50
40
30
20
10
0
EOM (mg/g TOC)
0
5
10
15
20
25
Cellulose (wt.%)
Adamów
Jóźwin IIB
Tomisławice
r2 = 0.67

Fig. 4

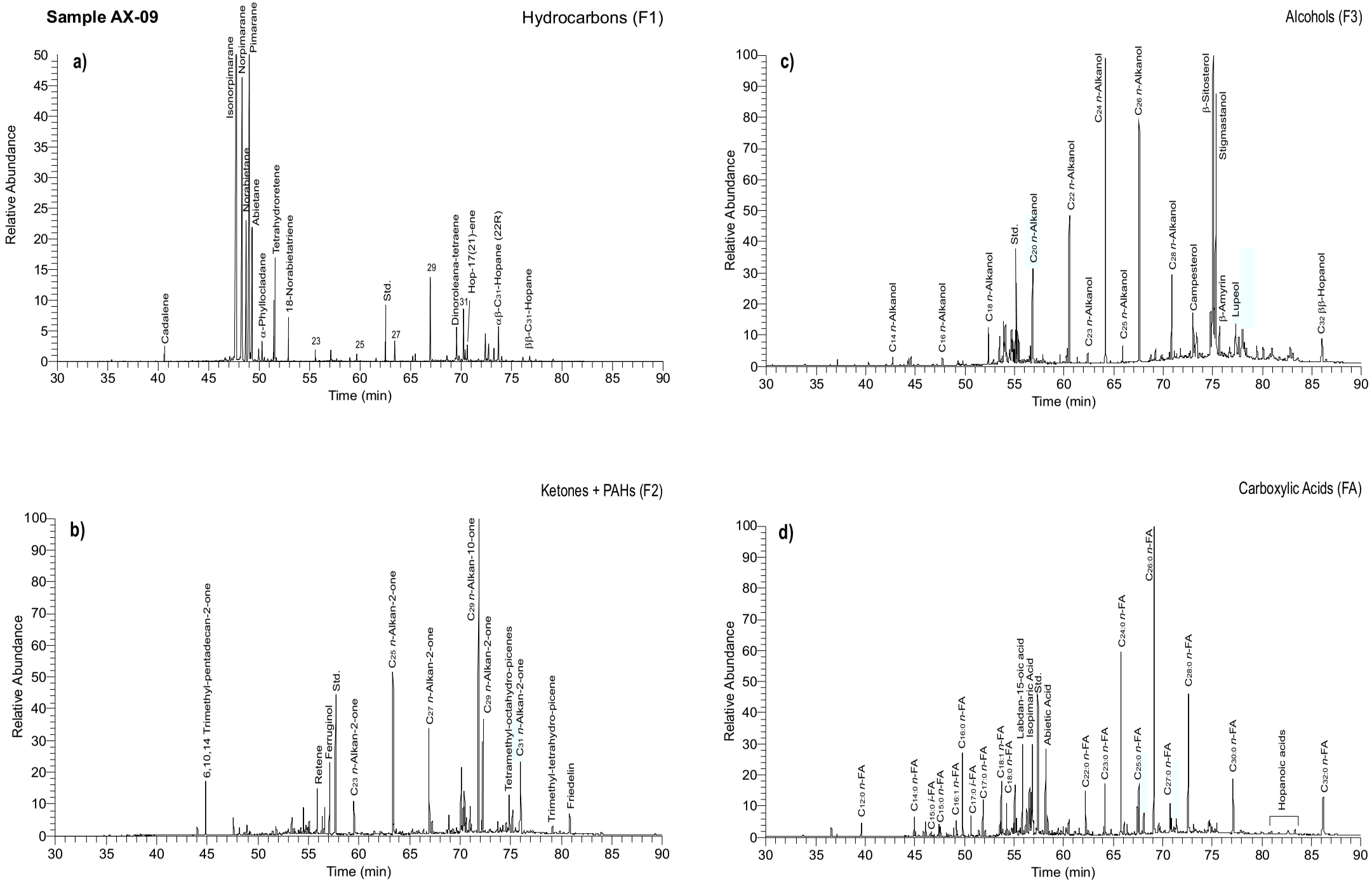
Sample AX-09
Hydrocarbons (F1)
a)
Relative Abundance
Time (min)
Cadalene
Isonorpimarane
Norpimarane
Pimarane
Norabietane
Abietane
α-Phyllocladane
Tetrahydroretene
18-Norabietatriene
23
25
Std.
27
29
Dinoroleana-tetraene
31
Hop-17(21)-ene
αβ-C31-Hopane (22R)
ββ-C31-Hopane
Alcohols (F3)
c)
C14 n-Alkanol
C16 n-Alkanol
C18 n-Alkanol
Std.
C20 n-Alkanol
C22 n-Alkanol
C23 n-Alkanol
C24 n-Alkanol
C25 n-Alkanol
C26 n-Alkanol
C28 n-Alkanol
Campesterol
β-Sitosterol
Stigmastanol
β-Amyrin
Lupeol
C32 ββ-Hopanol
Ketones + PAHs (F2)
b)
6,10,14 Trimethyl-pentadecan-2-one
Retene
Ferruginol
Std.
C23 n-Alkan-2-one
C25 n-Alkan-2-one
C27 n-Alkan-2-one
C29 n-Alkan-10-one
C29 n-Alkan-2-one
Tetramethyl-octahydro-picenes
C31 n-Alkan-2-one
Trimethyl-tetrahydro-picene
Friedelin
Carboxylic Acids (FA)
d)
C12:0 n-FA
C14:0 n-FA
C15:0 i-FA
C15:0 n-FA
C16:1 n-FA
C16:0 n-FA
C17:0 i-FA
C17:0 n-FA
C18:1 n-FA
C18:0 n-FA
Labdan-15-oic acid
Isopimaric Acid
Std.
Abietic Acid
C22:0 n-FA
C23:0 n-FA
C24:0 n-FA
C25:0 n-FA
C26:0 n-FA
C27:0 n-FA
C28:0 n-FA
C30:0 n-FA
Hopanoic acids
C32:0 n-FA

Fig. 5

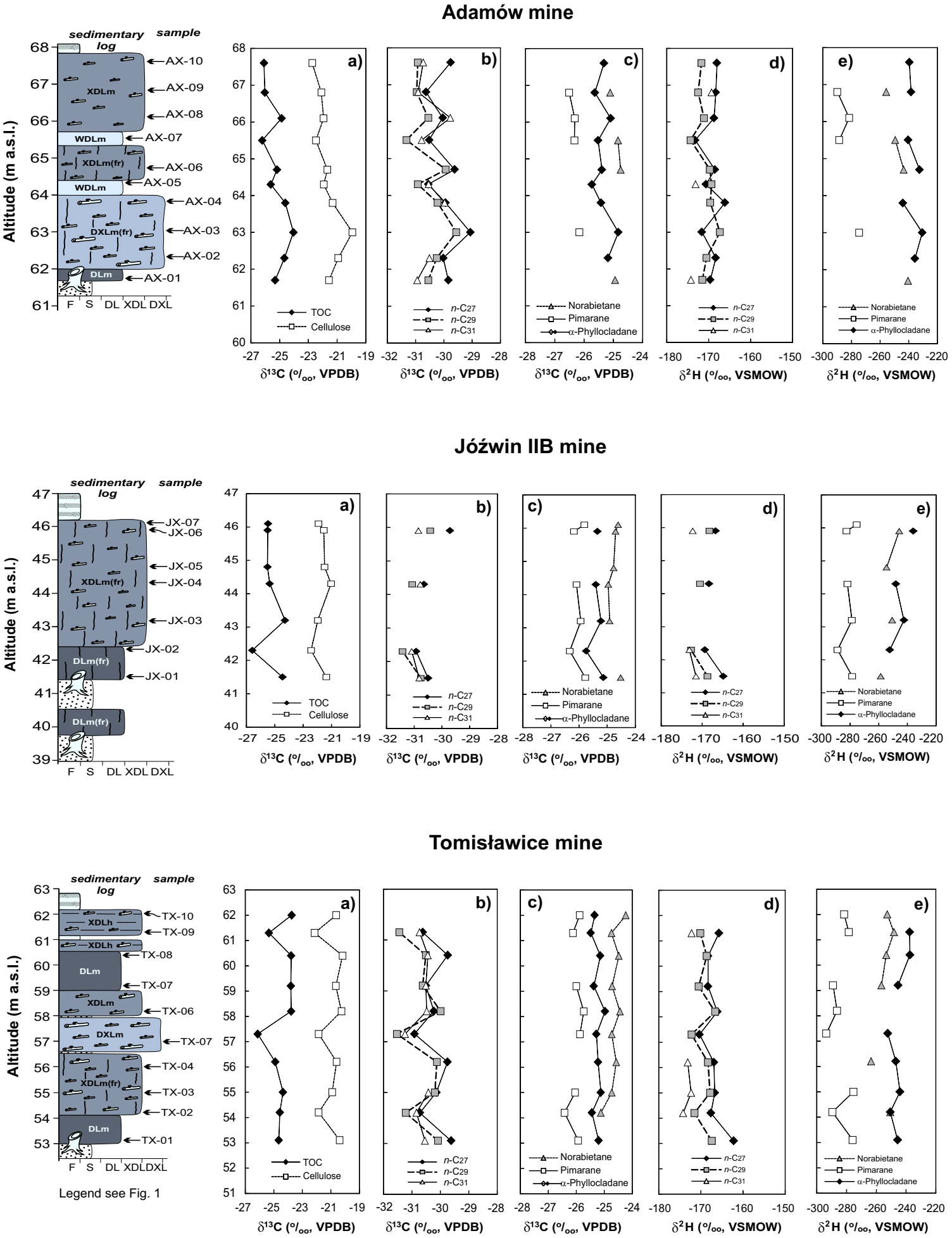
Adamów mine
sedimentary log
sample
Altitude (m a.s.l.)
XDLm
WDLm
XDLm(fr)
DXLm(fr)
DLm
AX-10
AX-09
AX-08
AX-07
AX-06
AX-05
AX-04
AX-03
AX-02
AX-01
F S DL XDL DXL
a)
b)
c)
d)
e)
TOC
Cellulose
n-C27
n-C29
n-C31
Norabietane
Pimarane
α-Phyllocladane
δ13C (o/oo, VPDB)
δ2H (o/oo, VSMOW)
Jóźwin IIB mine
JX-07
JX-06
JX-05
JX-04
JX-03
JX-02
JX-01
Tomisławice mine
XDLh
TX-10
TX-09
TX-08
TX-07
TX-06
TX-07
TX-04
TX-03
TX-02
TX-01
Legend see Fig. 1

Fig. 6

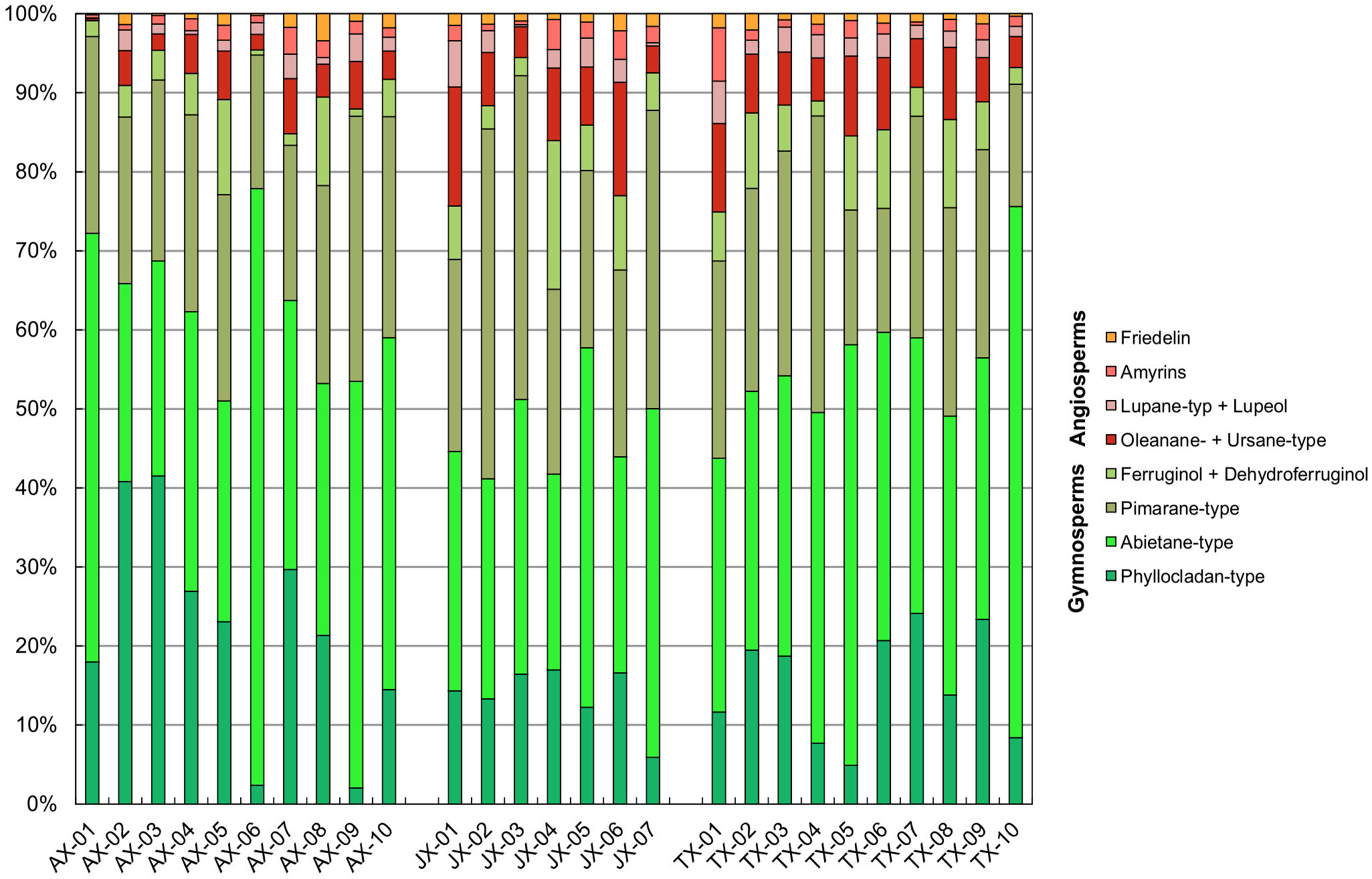
100%
90%
80%
70%
60%
50%
40%
30%
20%
10%
0%
AX-01
AX-02
AX-03
AX-04
AX-05
AX-06
AX-07
AX-08
AX-09
AX-10
JX-01
JX-02
JX-03
JX-04
JX-05
JX-06
JX-07
TX-01
TX-02
TX-03
TX-04
TX-05
TX-06
TX-07
TX-08
TX-09
TX-10
Angiosperms
Gymnosperms
Friedelin
Amyrins
Lupane-typ + Lupeol
Oleanane- + Ursane-type
Ferruginol + Dehydroferruginol
Pimarane-type
Abietane-type
Phyllocladan-type

Fig. 07

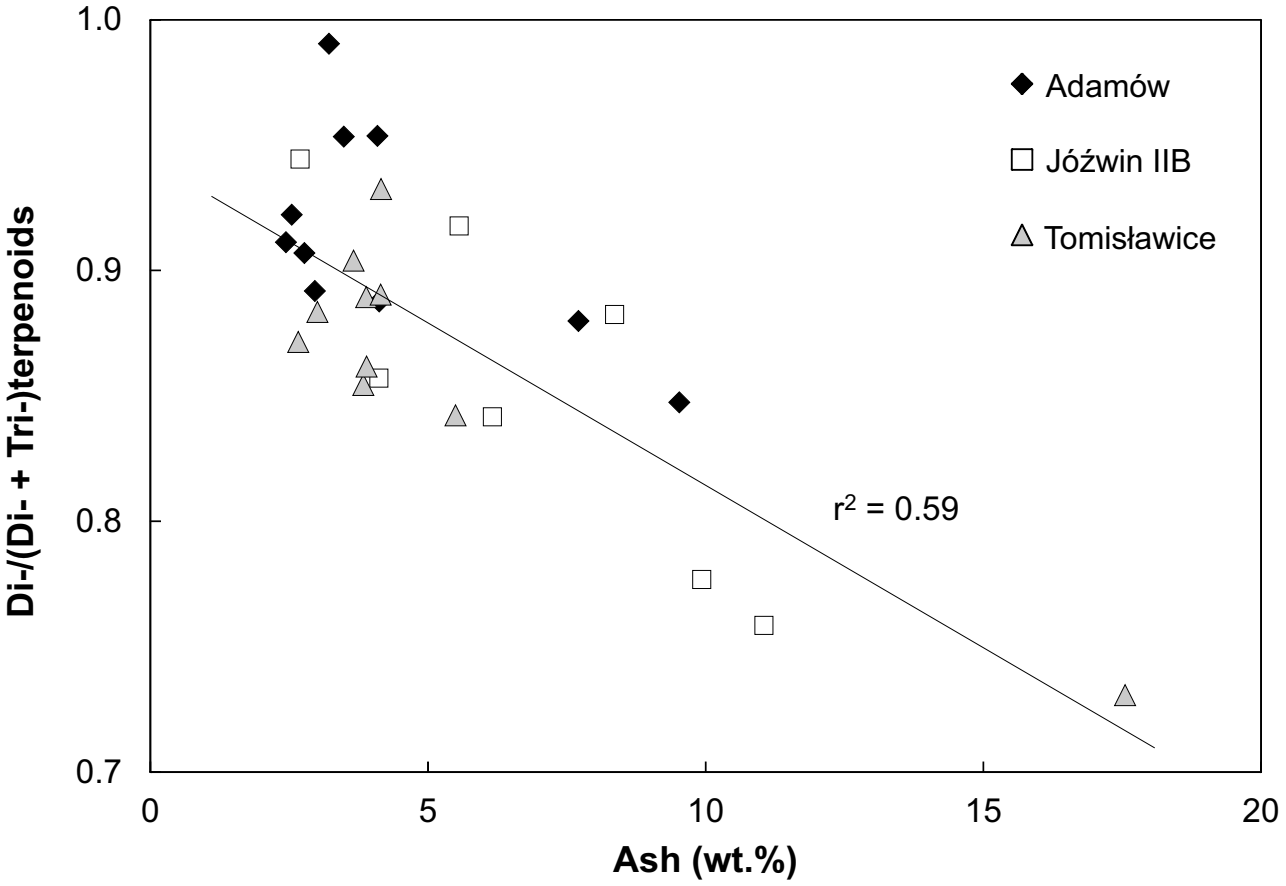
1.0
0.9
0.8
0.7
0
5
10
15
20
Di-/(Di- + Tri-)terpenoids
Ash (wt.%)
Adamów
Jóźwin IIB
Tomisławice
r2 = 0.59

Fig. 8

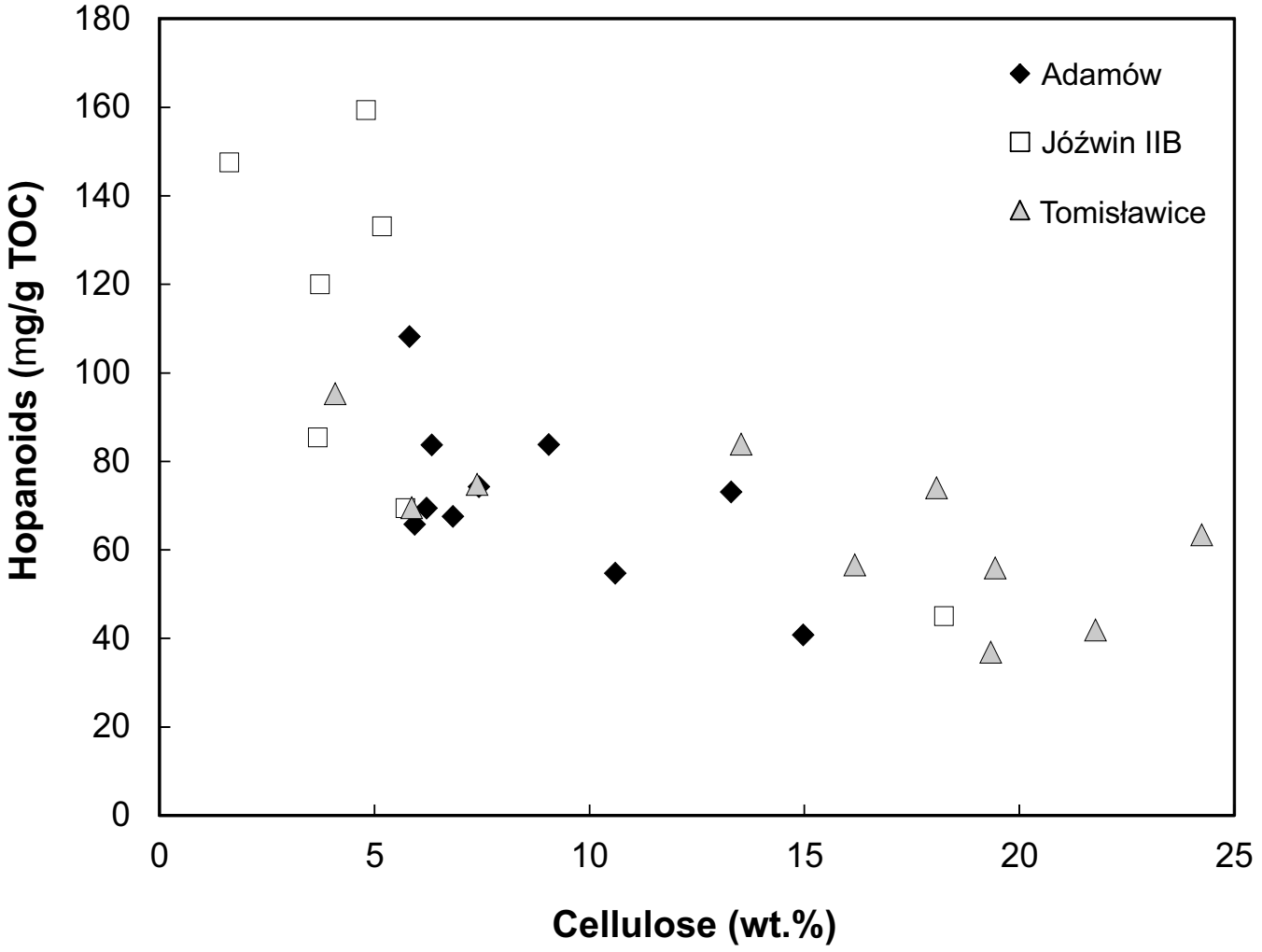
Hopanoids (mg/g TOC)
Cellulose (wt.%)
Adamów
Jóźwin IIB
Tomisławice
0
20
40
60
80
100
120
140
160
180
0
5
10
15
20
25

Fig. 9

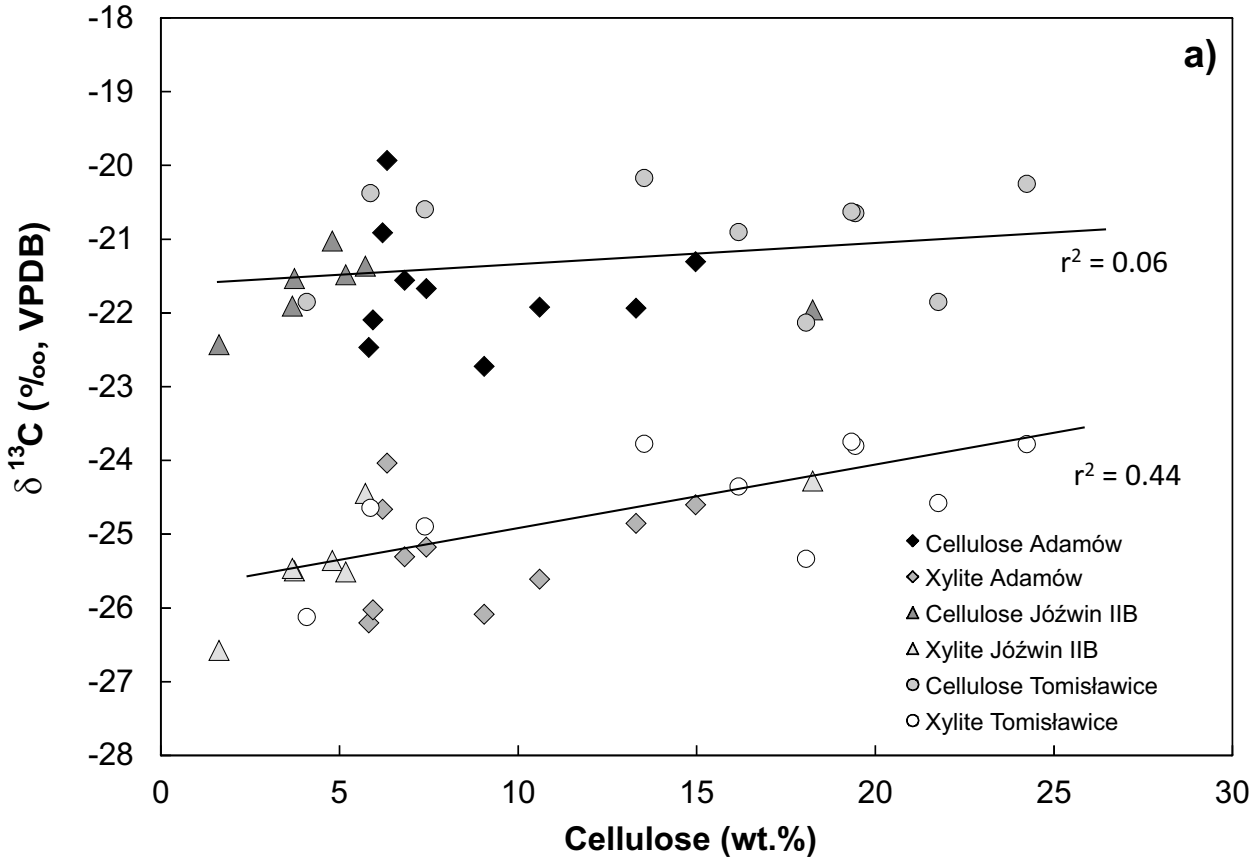
a)
δ 13C (‰, VPDB)
Cellulose (wt.%)
r2 = 0.06
r2 = 0.44
Cellulose Adamów
Xylite Adamów
Cellulose Jóźwin IIB
Xylite Jóźwin IIB
Cellulose Tomisławice
Xylite Tomisławice

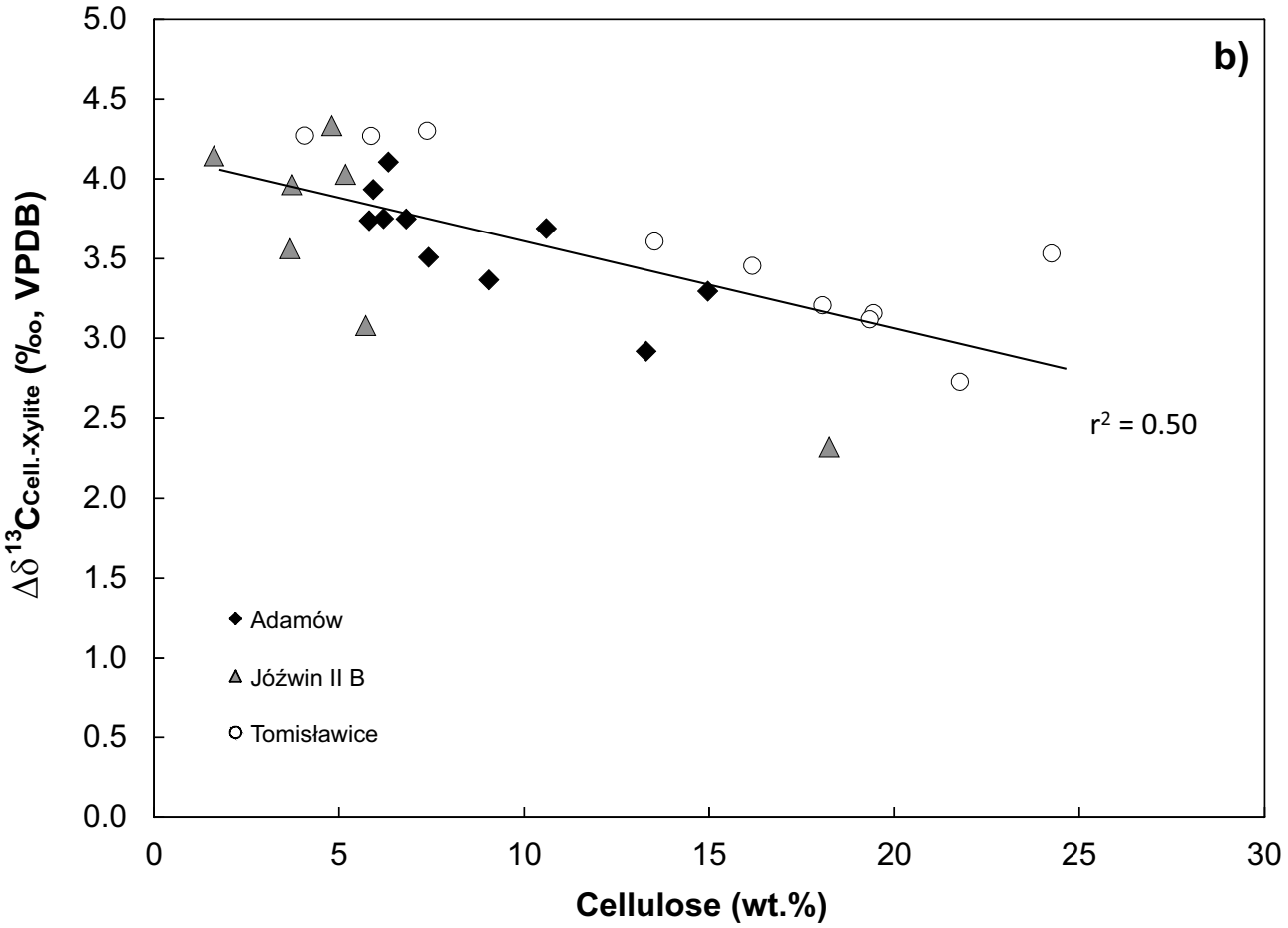
b)
Δδ 13CCell.-Xylite (‰, VPDB)
Cellulose (wt.%)
r2 = 0.50
Adamów
Jóźwin II B
Tomisławice

Fig. 10

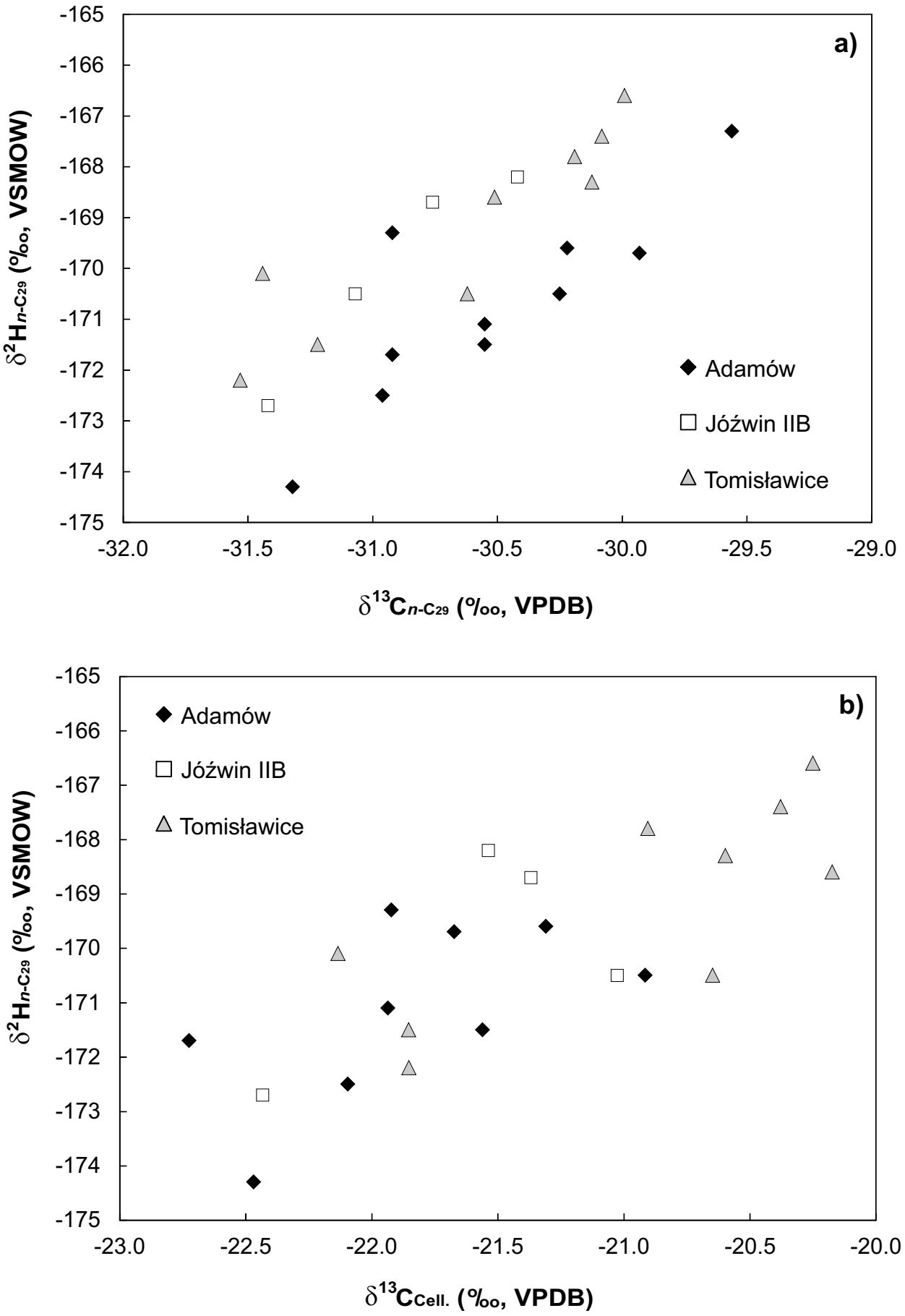
a)
-165
-166
-167
-168
-169
-170
-171
-172
-173
-174
-175
-32.0
-31.5
-31.0
-30.5
-30.0
-29.5
-29.0
δ2Hn-C29 (‰, VSMOW)
δ13Cn-C29 (‰, VPDB)
Adamów
Jóźwin IIB
Tomisławice
b)
-23.0
-22.5
-22.0
-21.5
-21.0
-20.5
-20.0
δ13CCell. (‰, VPDB)

Fig. 11